

# bradscholars

## Experimental investigation on flexural performance of steel-UHPC composite beams with steel shear keys

Item Type	Article
Authors	Zhang, Z.;Ashour, Ashraf;Ge, W.;Ni, Z.;Jiang, H.;Li, S.
Citation	Zhang Z, Ashour A, Ge W et al (2024) Experimental investigation on flexural performance of steel-UHPC composite beams with steel shear keys. Engineering Structures. 313: 118275.
DOI	<a href="https://doi.org/10.1016/j.engstruct.2024.118275">https://doi.org/10.1016/j.engstruct.2024.118275</a>
Rights	© 2024 Elsevier. Reproduced in accordance with the publisher's self-archiving policy. This manuscript version is made available under the CC-BY-NC-ND 4.0 license ( <a href="http://creativecommons.org/licenses/by-nc-nd/4.0/">http://creativecommons.org/licenses/by-nc-nd/4.0/</a> )
Download date	2026-05-20 07:35:24
Link to Item	<a href="http://hdl.handle.net/10454/19943">http://hdl.handle.net/10454/19943</a>

# Experimental study on flexural performance of steel-UHPC composite beams with steel shear keys

Zhiwen Zhang<sup>1</sup>, Ashraf Ashour<sup>2</sup>, Wenjie Ge<sup>1\*</sup>, Zenghao Ni<sup>1</sup>, Hongbo Jiang<sup>1</sup>, Yan Liu<sup>1</sup>

1. College of Civil Science and Engineering, Yangzhou University, Yangzhou 225127, China.
2. Faculty of Engineering and Informatics, University of Bradford, Bradford, BD71DP, UK.

**Abstract:** Test results of steel-ultra high performance concrete (UHPC) composite beams with welded steel shear keys (SSK) under four-point bending are presented, aiming to reduce the self-weight and cost of large span and heavy load structures. The effects of design parameters such as concrete slab strength, type, spacing and size of SSK, and concrete slab height and width on flexural performance of composite beams are studied. The experimental results show that increasing concrete strength, reducing SSK spacing, increasing concrete slab size, as well as using large-size SSK can all significantly improve the flexural performance of composite beams. Composite beams with welded SSK exhibited a maximum relative slip less than 4 mm, while counterpart with welded bolts had a maximum relative slip greater than 4 mm. Composite beams with SSK exhibited the highest load capacity and flexural stiffness, while the epoxy-treated composite beam had the lowest, and the welded bolt composite beam was in-between. The welded SSK is more effective in improving the interface shear performance of composite beams than the welded bolts, and can also improve the stiffness and load capacity of composite beams. Besides, a theoretical model is developed to calculate the ultimate flexural capacity of composite beams, and the calculated flexural capacity results well agree with the experimental results. It is expected that the research results can serve as a reference for the design and construction of steel-UHPC composite beams.

**Keywords:** composite beam; flexural performance; steel shear key; bearing capacity; deflection

## 1 Introduction

Composite beams have gained considerable popularity in the construction industry because of their exceptional load-bearing capacity and stiffness as well as their efficient use of materials and cost-effectiveness. The composite action between steel beams and concrete slabs is generally created using shear connectors, that are welded or mechanically fastened to the top flange of the steel beam and then embedded in the concrete slab during casting, allowing the steel beam and concrete slab to act together as a single unit, resulting in a stronger and stiffer composite element that can resist higher loads and span longer distances than either material alone. Moreover, composite structures can reduce construction workload and decrease steel section size, allowing more headroom in buildings and reducing size and cost of foundations [1-2]. However, with the widespread use of long-span and

heavy-duty structures, traditional steel-normal strength concrete (NSC) composite beams are disadvantageous due to their inherent weight, high manufacturing costs, and waste of steel performance [3-4].

Ultra high performance concrete (UHPC) is an advanced type of concrete that has superior strength, durability, light weight and ductility compared to traditional concrete. [5]. It is widely used in the construction of high performance structures, including high-rise buildings, bridges, offshore structures, national defense engineering and other applications [6] as well as achieving high-rise, light-weight, long-span, and long-life requirements [7]. Due to the widespread use of UHPC, steel-UHPC composite structures have gradually attracted the attention of construction industry. The combination of UHPC and section steel provides excellent mechanical properties and superior ductility [8].

Studies on the flexural performance of steel-UHPC composite beams are limited in the literature. The flexural performance of steel-UHPC-NSC composite beams in the negative moment zone was experimentally investigated by Lu et al. [9]. The results show that the failure mode of the specimens in the push-out test is crushing and spalling of the concrete at the stud root. Damage degree and damage range of UHPC specimens, however, are significantly smaller than those of composite NSC-UHPC specimens. Zhao et al. [10] investigated the shear properties of steel-UHPC composite beams to take full advantage of the strong tensile properties of UHPC. Test results indicated that the shear performance of composite beams was significantly related to the shear-span ratio, concluding that shear capacity decreased by 30.5%, while ductility increased by 24.2%, as the shear-span ratio increased from 1.33 to 2.33. Zhu et al. [11-12] investigated the flexural behavior of steel-UHPC composite beams in waffle bridge deck, showing that the transverse reinforcement ratio does not affect the bearing capacity of composite beams, but it has a profound effect on the ultimate deformation. An experimental and numerical study was conducted on steel-UHPC-steel sandwich composite beams with novel enhanced C-channel connectors, which was proposed by Yan et al. [13-14]. According to the study, the new grooved connector has extremely high shear resistance and bonding efficiency. The thickness of steel panels has a significant impact on the bearing capacity of composite beams, while the spacing of groove connectors has a relatively small effect.

The advancements in production technology have led to a continuous improvement and innovation of steel-concrete composite beams. The prefabricated assembly type has gradually replaced the traditional cast-in-place composite beams due to its inherent shortcomings, such as wet operations on site, the prolonged construction period, and the resulting negative effects on construction quality caused by the environment. To ensure a stable combination and synergy between steel beams and concrete slabs, shear bonds play an important role. To address the issue of uneven

failure of bolt shear keys with a uniform arrangement [15], a clustered arrangement of bolt shear keys has been implemented in composite beams instead of the conventional uniform arrangement [16-18]. Through the push-out test, Wang et al. [19] found that the group nail effect has a slight influence on the ultimate shear strength of the bolt, but it clearly affects the interface slip. Prefabricated specimens have a lower ultimate strength than cast-in-place specimens, while their interface slip is higher by 17% [19]. UHPC replaces high-strength grouting material for post-filling, resulting in an increase in shear strength of 16%, the 50% reduction in slip, and the occurrence of no obvious cracks. Fang et al. [20] investigated the flexural performance of steel-prefabricated UHPC composite beams embedded in UHPC shear pockets. The results indicated that the cracking and failure modes of composite beams are greatly influenced by the type of precast concrete and degree of shear connection. The crack resistance, ultimate strength, and ductility of composite beams constructed using UHPC panels are higher than those constructed using NSC panels. Yoo et al. [21] studied the flexural performance of eight steel-UHPC composite beams without upper flanges in order to improve the economy of materials. The experimental results showed that specimens with a large bolt spacing generate a greater number of axial cracks in the UHPC plate. Consequently, the strength, dimension and the degree of shear connection of concrete and steel beam affect the failure modes and performance of steel-UHPC composite beam.

Currently, the bolt shear key is the main method to enhance ductility of composite beams. Nevertheless, the initial slip is often influenced by the allowable error of the bolt hole diameter, resulting in low ultimate load and bending stiffness. Additionally, if the shear resistance of the shear key is low, the composite beam will fail prematurely due to bolt shearing. In this paper, a novel steel-UHPC composite beam with steel shear keys (SSK) is designed to reduce the self-weight and engineering costs of long-span and heavy load structures, as shown in Fig. 1. Here, the bolt is replaced with angle steel pre-welded on the top of the upper flange of the steel beam, preventing any damage caused by pre-drilling of the steel beam as well as making construction straightforward. Four-point bending tests were conducted to analysis the failure modes, load-deflection response, load-strain response and load-slip response of the steel-UHPC composite beams with welded SSK. The effects of design parameters such as concrete slab strength, spacing of SSK, height and width of concrete slab, and types of shear keys on flexural performance of composite beams were investigated. Besides, a theoretical model is developed to calculate the moment capacity of steel-UHPC composite beams. It is expected that this study will provide technical support for the application of steel-UHPC composite beams in engineering structures as well as provide a reference for their design and construction.

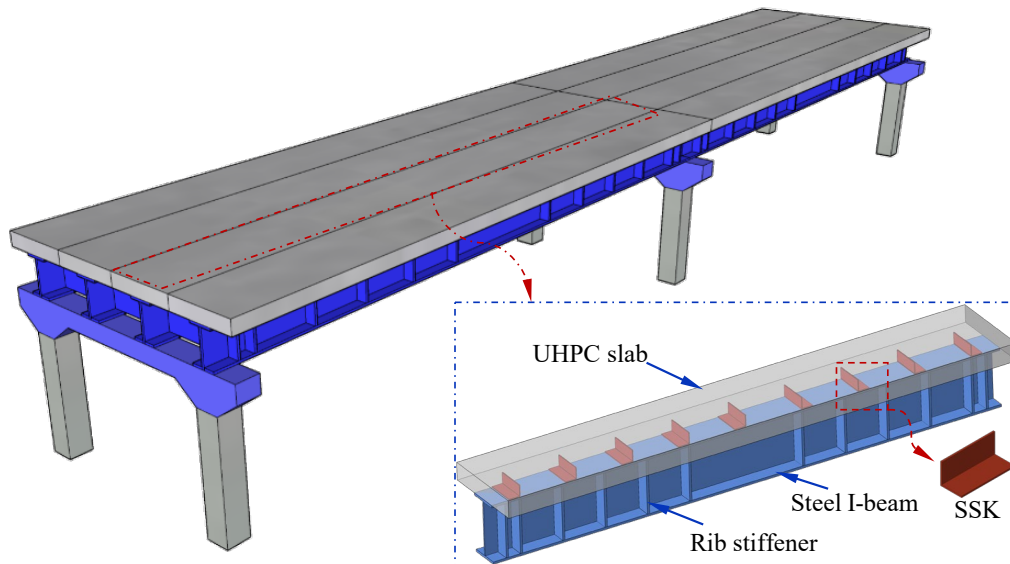


Fig. 1 Application of the steel-UHPC composite beam with SSK

## 2 Material properties

Here, NSC and UHPC are prepared in accordance with Chinese codes JGJ 55-2019 [22] and GB/T 31387-2015 [23], respectively. Table 2 presents the mass ratios of various ingredients used in NSC and UHPC. NSC and UHPC are both made with manufactured sand of an average particle size of 50  $\mu\text{m}$ , and Portland cement of grades PO 42.5 and PO 52.5 cements were used, respectively. In NSC, stones with particle size of 5 mm to 20 mm were utilized as the coarse aggregate. The active mineral admixtures employed in UHPC include 400 mesh silica fume, slag powder grade S95, and fly ash grade II, with their respective chemical composition outlined in Table 1. Additionally, copper-plated straight steel fibers having a diameter of 0.22 mm, a length of 13 mm, and a tensile strength greater than 2850 MPa were also incorporated in producing UHPC. Local tap mixing water and polycarboxylate superplasticizer with a solid content of 20% and a water reduction rate of 32% was employed.

The UHPC paste was prepared by the cement paste mixer NJ-160. The cementitious materials, including cement, silica fume, slag and fly ash, were initially accurately weighed by an electronic scale (maximal measuring weight is 3.0 kg, measurement accuracy is 0.1 g). Then, the cementitious materials were poured into the mixing pot and a solution of local tap water and water reducer was added. The ingredients were mixed for 120 seconds at a low speed (rotation around its own axis at a speed of  $140 \pm 5$  r/min and revolution around the axis of mixing pot at a speed of  $62 \pm 5$  r/min) and held for 15 seconds, 120 seconds at a high speed (rotation around its own axis at a speed of  $285 \pm 10$  r/min and revolution around the axis of mixing pot at a speed of  $125 \pm 5$  r/min), and held for 15 seconds. Then, the previous steps were repeated once again. Seamless metallic cone with smooth inner wall having a height of 60 mm, lower diameter of 60 mm and upper diameter of 36 mm, was used to test the fluidity of UHPC paste.

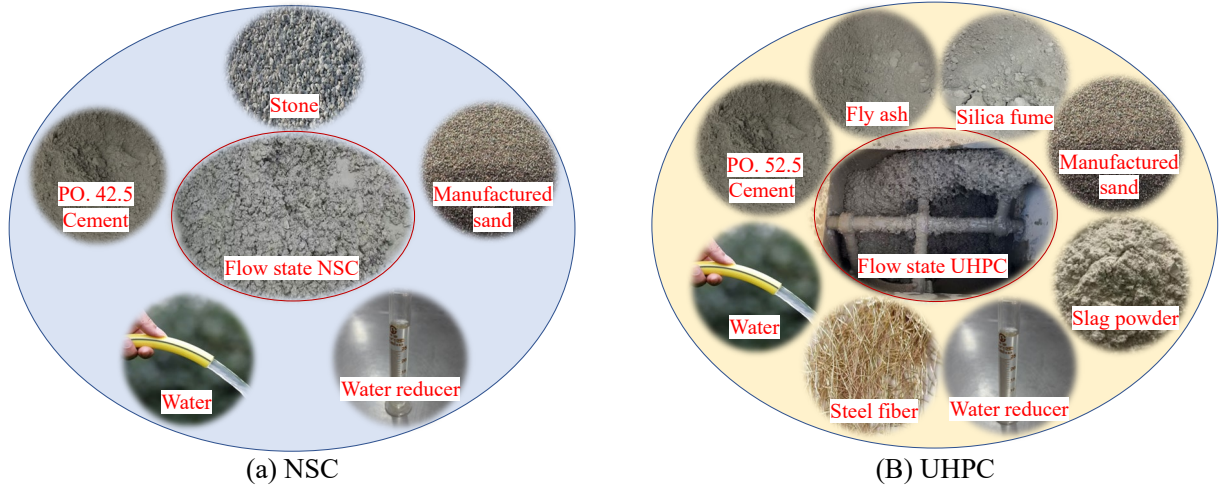


Fig. 2 Raw material of NSC and UHPC

Tab. 1 Compositions of mineral admixtures (unit: %)

No.	SiO <sub>2</sub>	Al <sub>2</sub> O <sub>3</sub>	CaO	MgO	Fe <sub>2</sub> O <sub>3</sub>	Na <sub>2</sub> O	TiO <sub>2</sub>
Silica fume	96.74	0.32	0.11	0.10	0.08	0.09	/
Slag powder	32.80	15.36	37.12	8.52	0.74	/	1.95
Fly ash	54.76	24.56	4.85	0.10	6.54	/	1.85

Tab. 2 Mixture proportions by weight of NSC and UHPC

No.	w/b	Cement	Sand	Stone	Slag powder	Silica fume	Fly ash	$\rho_s$ (%)	Superplasticizer (%)
C40	0.42	1.0	1.64	2.67	/	/	/	/	1.05
C50	0.32	1.0	1.11	2.59	/	/	/	/	1.2
UHPC	0.19	0.55	1.2	/	0.1	0.25	0.1	1.0	1.5

Note: w/b is the water-binder ratio,  $\rho_s$  is the volume fraction of steel fiber.

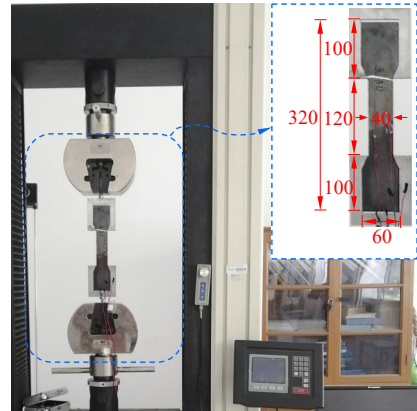
Mechanical tests of NSC and UHPC were conducted in accordance with Chinese codes GB/T 50081-2019 [24] and T/CBMF 37-2018, T/CCPA 7-2018 [25], respectively. Three cubic concrete specimens (100 × 100 × 100 mm) were prepared for compression testing, along with three dumbbell-shaped concrete specimens for tensile testing (Fig. 3b). These specimens were cured in the same environment as the main composite beams. Table 3 shows the basic mechanical properties of UHPC and NSC, where the cubic compressive strength  $f_{cu}$  and the axial tensile strength  $f_t$  are test values, whereas the axial compressive strength  $f_c$  and elastic modulus  $E_c$  are calculated values in according to [26-28].

The steel beam and SSK are made from Q235 steel, while the bolt shear keys are made from M10 bolts. For the tensile tests of Q235 steel, three samples were taken from the flange and web of the steel beam, and cut into standard dimension according to the Chinese code GB/T228.1-202 [29]. The uniaxial tensile test of the bolt shear key was carried out by using a smooth round screw with a diameter of 10 mm and a length of 80 mm. Table 4 shows the basic mechanical properties of Q235 steel and M10 bolts, where the yield strength  $f_y$  and the ultimate tensile strength  $f_u$  are determined

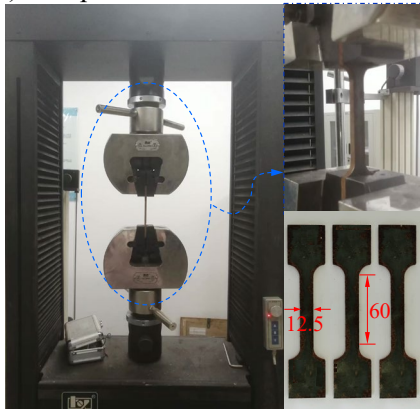
experimentally, while the elastic modulus  $E_s$  values are calculated in accordance to [29].



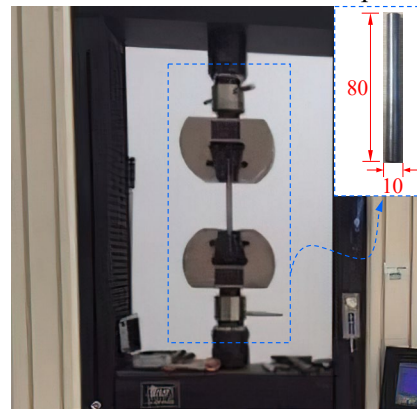
(a) Compression tests for cubic concrete



(b) Axial tensile test for dumbbell-shaped concrete



(c) Tensile test for Q235 steel



(d) Tensile test for M10 bolt

Fig. 3 Mechanical properties test

Tab. 3 Mechanical Properties of NSC and UHPC

No.	$f_{cu}$ (MPa)	$f_c$ (MPa)	$f_t$ (MPa)	$E_c$ (GPa)
C40	45.8	34.8	2.8	33.8
C50	57.5	43.7	3.2	35.7
UHPC	106.4	93.6	7.9	43.2

Tab. 4 Mechanical Properties of Q235 steel and M10 bolt

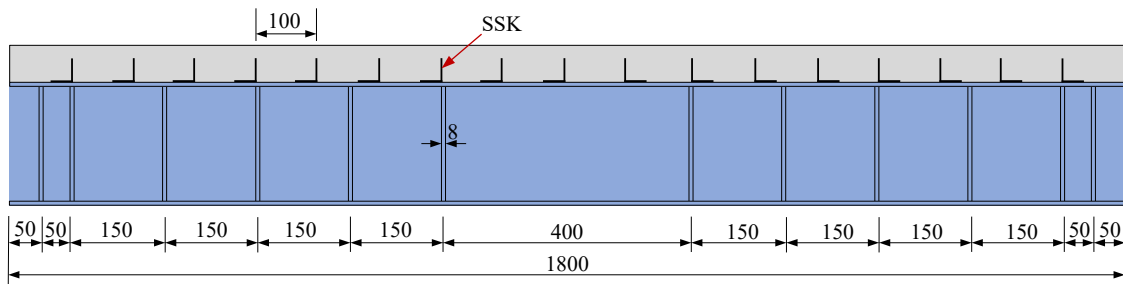
No.	Thickness of steel (mm)	Diameter of M10 bolt (mm)	$f_y$ (MPa)	$f_u$ (MPa)	$E_s$ (GPa)
Q235 steel	3	/	258.4	403.8	202
	4	/	264.5	412.5	204
	5	/	261.5	417.2	203
	8	/	278.8	406.9	206
M10 bolt	/	10	405.8	467.2	208

According to the testing report provided by the manufacturer, the epoxy resin (E-44) has a tensile strength of 40.5 MPa, a tensile elastic modulus of 3.4 GPa, a shear strength of 12.7 MPa, a bond strength of 3.7 MPa with concrete (cohesive failure), and an elongation of 2.3%. It has a curing time of 4 to 6 hours, and a temperature resistance of  $-60\text{ }^{\circ}\text{C} \sim 120\text{ }^{\circ}\text{C}$ .

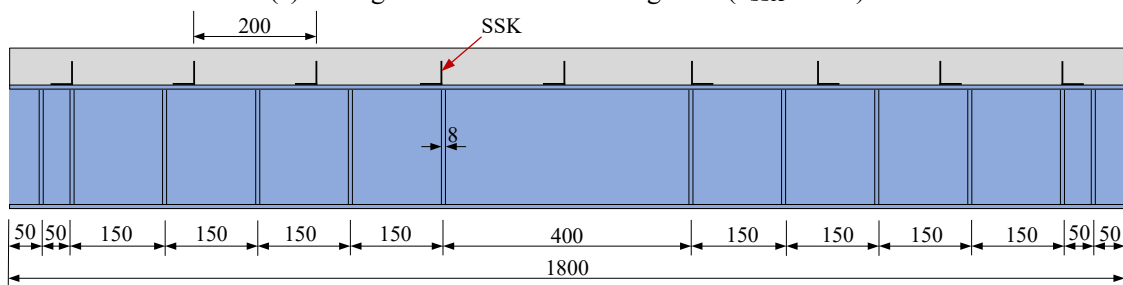
### 3 Experimental programs

#### 3.1 Design of test specimens

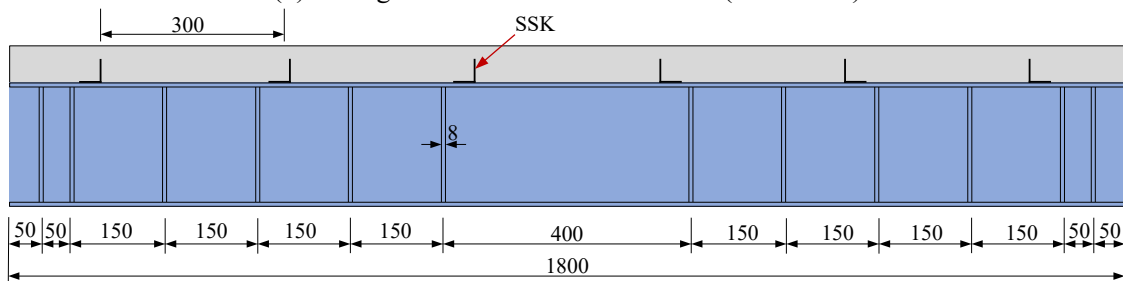
In total, ten composite beams were tested in this investigation, covering a wide range of parameters including the concrete type of slabs, concrete slab flange width and depth, type and spacing of shear connectors and the dimensions of SSK, as shown in Fig. 4 and listed in Table 5. All specimens have a length of 1800 mm, with pure bending section spanning 400 mm, and bending-shear sections spanning 650 mm. The size ratio of prototype to test model is 2:1. The dimensions of the I-shaped steel beams for all the specimens are  $184 \times 100 \times 5 \times 8$  mm ( $h_w \times b_s \times t_w \times t_f$ ). S1 is considered as a control specimen, having a UHPC slab with a cross-sectional dimension of  $60 \times 200$  mm ( $b_c \times h_c$ ), spacing and size of SSK of 200mm and  $3 \times 40 \times 40$  mm ( $t_s \times b_s \times h_s$ ). Specimens S2 and S3 are identical to S1 but the concrete slab was made from NSC having concrete class C40 and C50, respectively. Specimens S1~S8 utilized welded SSKs with different size and spacing, while specimen S9 employs bolt shear keys with a diameter of 10 mm and a spacing of 200 mm. In specimen S10, the composite interface is wet-bonded using epoxy resin (E-44) [30]. The web of each specimen is stiffened vertically by welding 8 mm thick steel plates with a 10 mm fillet weld throughout the stiffener height.



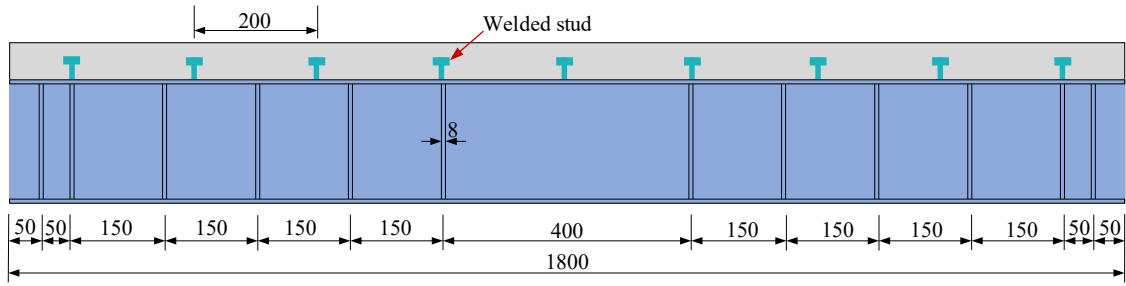
(a) Arrangement details of welded SSK ( $d_{SSK} = 100$ )



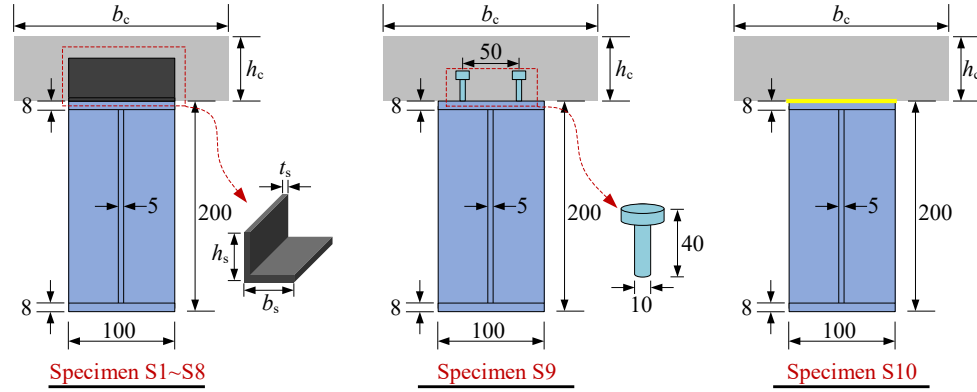
(b) Arrangement details of welded SSK ( $d_{SSK} = 200$ )



(b) Arrangement details of welded SSK ( $d_{SSK} = 300$ )



(d) Arrangement details of welded bolts



(e) Dimensions of mid-span cross-section

Fig. 4 Geometric details of steel-UHPC composite beams (unit: mm)

Tab. 5 Design parameters of steel-UHPC composite beams

No.	Types of concrete	Types of shear keys	$b_c \times h_c$ (mm)	$t_{ssk} \times b_{ssk} \times h_{ssk}$ (mm)	Spacing of shear keys (mm)
S1	UHPC	SSK	200 × 60	3 × 40 × 40	200
S2	C40	SSK	200 × 60	3 × 40 × 40	200
S3	C50	SSK	200 × 60	3 × 40 × 40	200
S4	UHPC	SSK	200 × 60	4 × 50 × 50	200
S5	UHPC	SSK	200 × 60	3 × 40 × 40	100
S6	UHPC	SSK	200 × 60	3 × 40 × 40	300
S7	UHPC	SSK	300 × 60	3 × 40 × 40	200
S8	UHPC	SSK	200 × 75	3 × 40 × 40	200
S9	UHPC	Bolts	200 × 60	/	200
S10	UHPC	Epoxy resin	200 × 60	/	/

### 3.2 Specimen fabrication

Figure 5 shows the fabrication procedures of steel-UHPC composite beams. First, steel beams were cold welded with vertical stiffeners, angle steel, and bolt shear keys. Second, the upper flange of the section steel was polished, then wiped by alcohol, and strain gauges were attached. For specimens S1 ~ S9, concrete was poured following the completion of the formwork, whereas, epoxy resin glue was applied to the upper flange of specimen S10, and concrete was poured before the glue layer fully cured. The wet concrete was leveled after it has been poured. Finally, the formwork was removed after 15 days of natural curing.

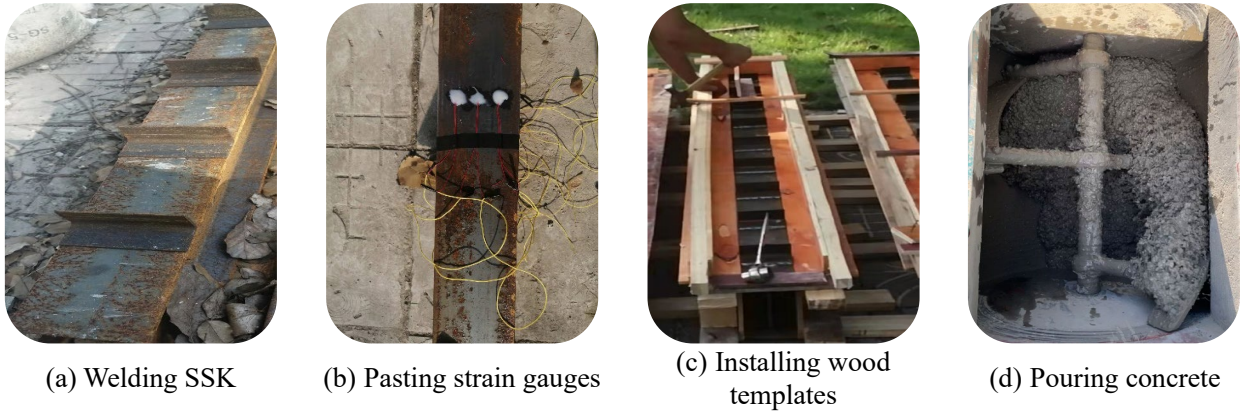


Fig. 5 Prefabrication procedure of composite beams

### 3.3 Test setup and measurements

Figure 6 illustrates the loading arrangement of four-point bending test for all composite beams. A hydraulic jack with a capacity of 1000 kN was adopted to apply the vertical load that was equally distributed to the rollers 200 mm away from the middle span of the composite beam, using a load distribution beam. To ensure that the loading device and measuring equipment being worked properly, the test specimen was preload first. A load control method with a loading level of 20 kN was initially adopted until the specimen cracked, subsequently increased to 40 kN. The loading process was terminated once the specimen was damaged (fracture of bottom steel or crushing of upper concrete) and the load dropped below 85% of the ultimate load.

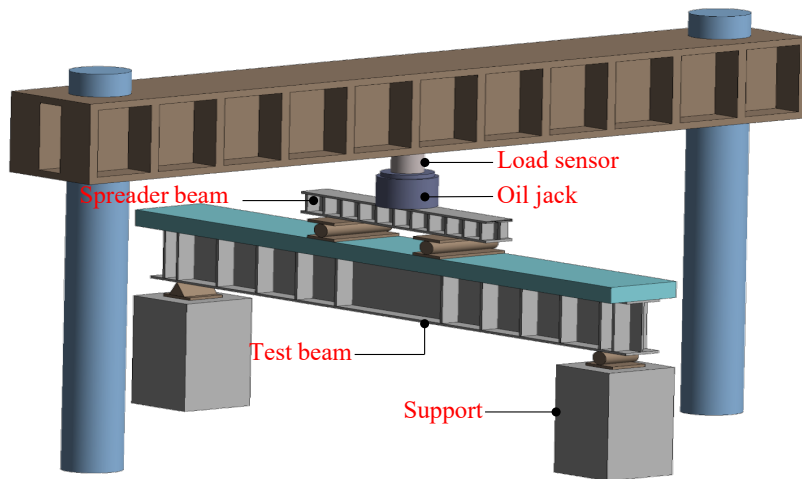


Fig. 6 Test setup

The layout of all measurements is shown in Fig. 7. In this study, seven displacement transducers were used to measure the deformation of the bottom of the composite beam along its length and the settlement at the two supports. For the measurement of the relative slip between the concrete slab and the steel beam, as well as the end slip of the concrete slab, a total of 10 dial gauges were used. During the test, the data acquisition system "TDS 530" was used to record all measured data, including load, displacements, and strains.

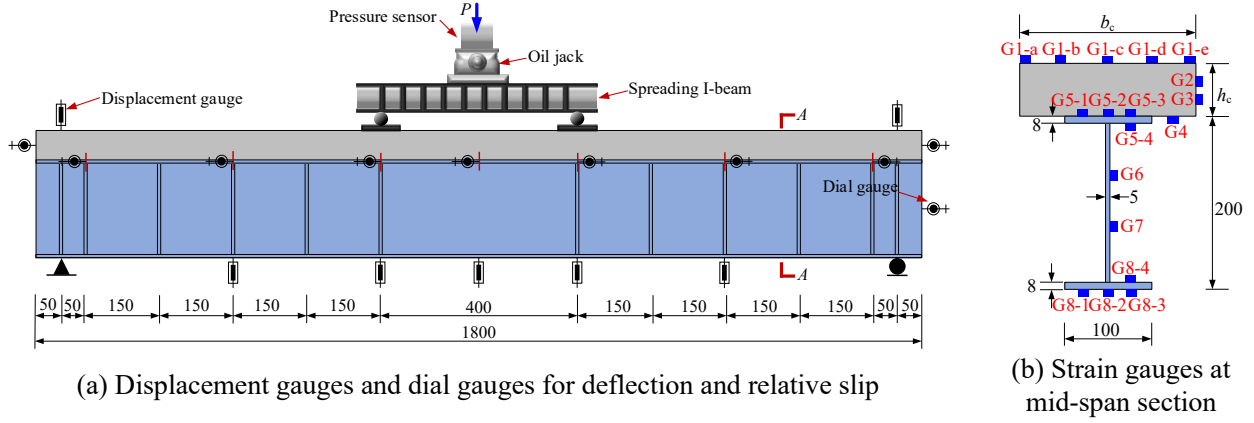


Fig. 7 Layout of the measurements (unit: mm)

## 4 Experimental results

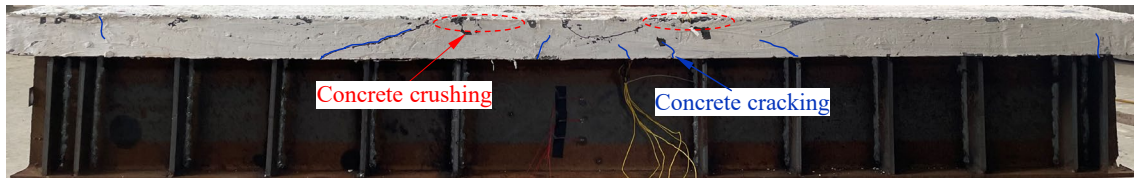
In this section, the failure modes, load-deflection, load-strain, and load-slip responses are presented and comprehensively analyzed. Besides, the effects of design parameters such as strength of concrete slab, spacing of SSK, height and width of concrete slab, and types of shear keys on flexural performance of composite beams are discussed.

### 4.1 Experimental phenomenon

Figure 8 illustrates the crack patterns of all specimens. For specimens S1 and S9, the concrete slab cracked first at the bottom of the pure bending section. As soon as the steel section had reached the yield point, more cracks gradually propagated in the bending and shearing regions, and the number of cracks significantly increased, resulting in a gradual reduction of the beam load resistance. Following the concrete slab being crushed, the section steel yielded, and the load began to fall after reaching the ultimate load, causing a typical flexural failure. The presence of vertical stiffeners in composite beams prevented buckling of the steel beam web during the bending test. Despite the crushing of concrete, composite beams exhibited good ductility. It is noteworthy that the welded shear keys of all specimens did not fail during the bending test, indicating that the composite interfaces of S1~S9 all have good shear performance and good composite action. Since the bridging connection [31] was provided by the steel fibers in UHPC matrix, the cracking of UHPC-steel composite beams S1 and S9 is effectively restrained. Because of the strain hardening behavior [31] of UHPC mixed with steel fibers, the fibers slowly being pull out from the UHPC matrix before the composite beam fails.

For specimen S10, the debonding failure along the interface between the concrete slab and steel beam occurred before cracking of concrete. The concrete slab and steel beams are no longer acting together as one composite element, and the internal forces are redistributed within the beam cross-section. As a result, the concrete slab and the steel beam overlap each other, with both having compression and tension zones, while the composite beam was still able to undergo a significant

amount of deformation. It is evident that the relative slip between the concrete slab and the steel beam becomes more apparent as the load increases. Vertical flexural cracks developed at the point of loading until they penetrated the concrete slab, that was sheared at this point, causing the load to drop suddenly, and the composite beam finally collapsed.



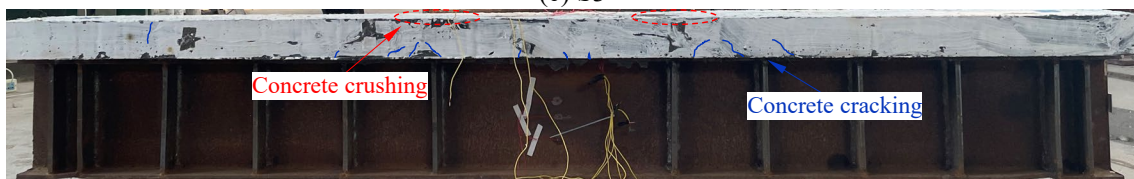
(a) S1



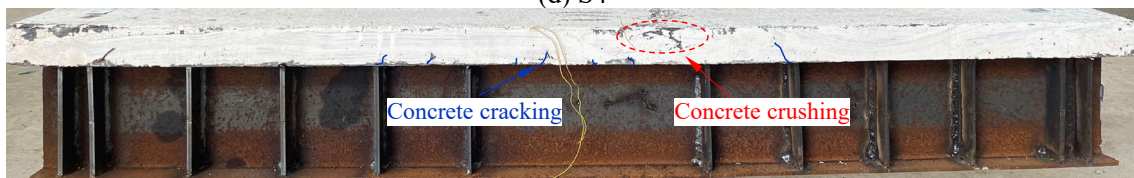
(b) S2



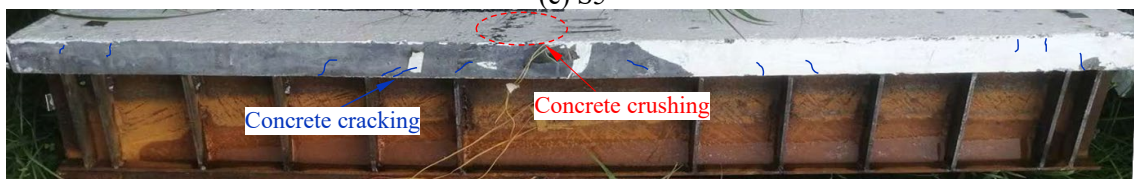
(c) S3



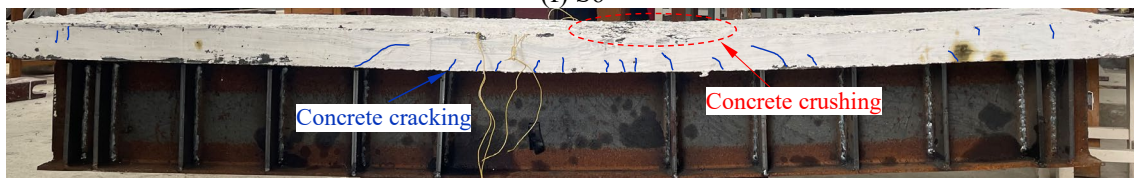
(d) S4



(e) S5



(f) S6



(g) S7



(h) S8

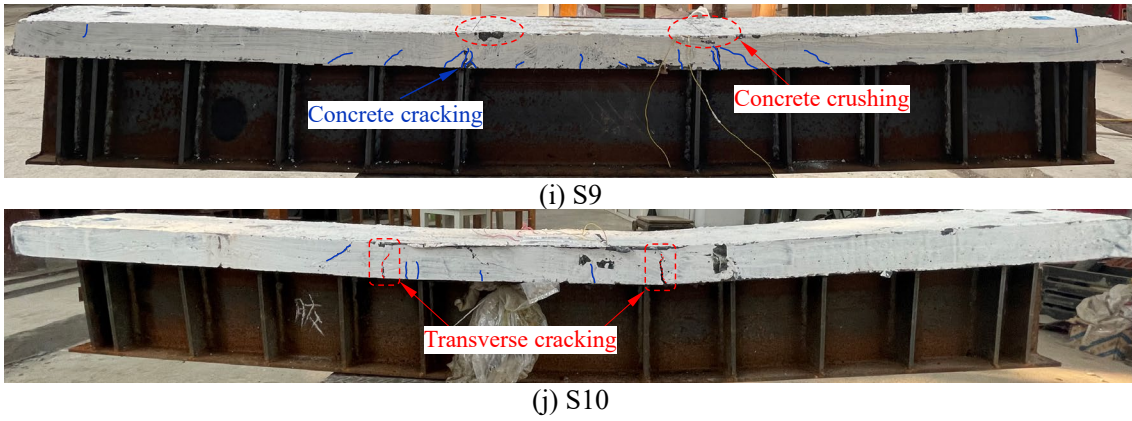
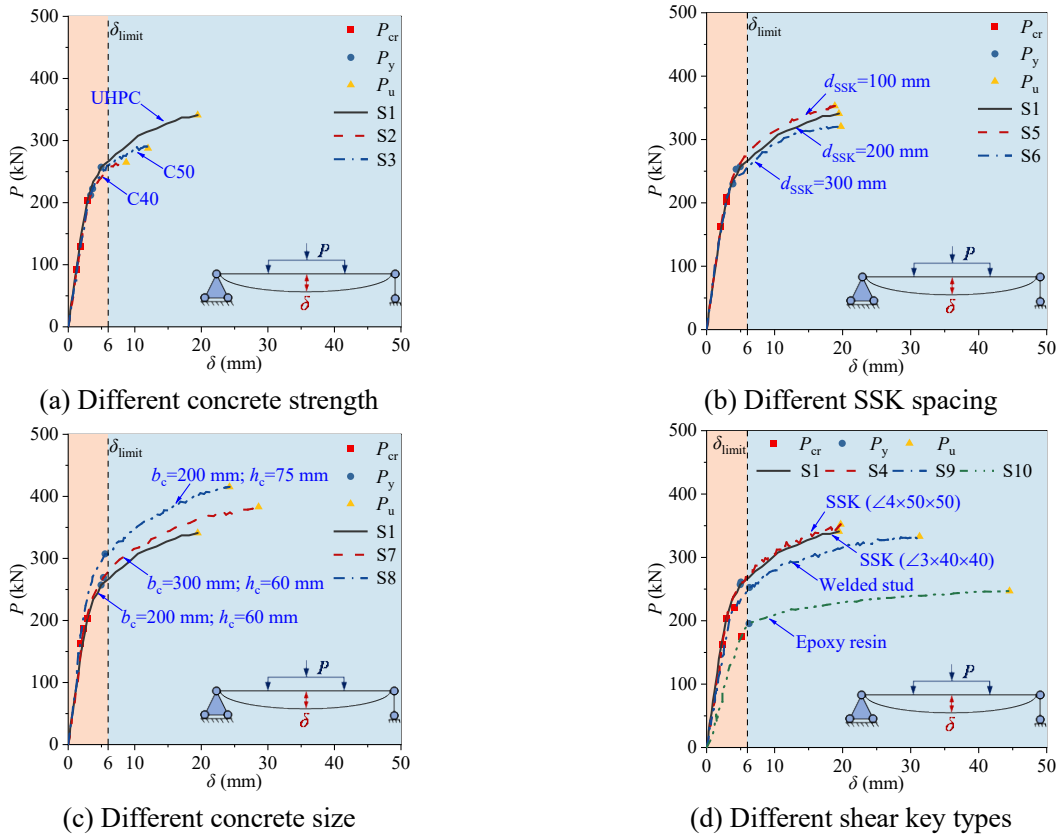


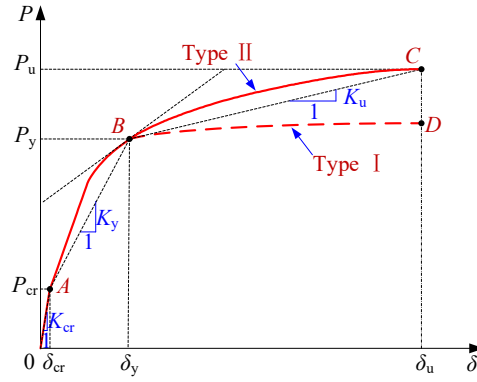
Fig. 8 Crack patterns for composite beams

## 4.2 Load-deflection response

### 4.2.1 Load-deflection curve

The load-mid-span deflection curves of all specimens are shown in Fig. 9, and the test results are listed in Table 6, where,  $P_{cr}$  and  $\delta_{cr}$  are cracking load and corresponding deflection;  $P_y$  and  $\delta_y$  are yield load and corresponding deflection;  $P_u$  and  $\delta_u$  are the ultimate load and corresponding deflection;  $s_R$  and  $s_L$  are the maximum slip at the left and right ends of the concrete slab. Here, the yield point of the curve is determined according to the "farthest point method" proposed by Feng et al. [32]. As the specimens was tested under load control, the load of the composite beam dropped rapidly, upon crushing of concrete. Thus, the load and deflection corresponding to the peak point are directly defined as the ultimate load and deflection, respectively.





(e) Generalized load-deflection curves  
Fig. 9 Load-deflection curves

Tab. 6 Comparison of characteristic load and deflection, slip and failure pattern

No.	$P_{cr}$ (kN)	$\delta_{cr}$ (mm)	$P_y$ (kN)	$\delta_y$ (mm)	$P_u$ (kN)	$\delta_u$ (mm)	$s_L$ (mm)	$s_R$ (mm)	Failure mode
S1	202.9	2.9	257.2	4.9	341.0	19.5	2.6	2.7	Bending
S2	92.2	1.5	202.0	3.9	264.8	8.7	1.3	1.2	Bending
S3	129.5	1.9	209.4	4.0	287.5	12.0	1.7	1.7	Bending
S4	212.0	2.4	284.1	5.0	372.2	18.7	2.7	2.6	Bending
S5	221.9	2.6	262.2	4.8	353.0	17.8	2.3	2.4	Bending
S6	210.6	3.6	247.0	5.1	302.5	24.7	3.1	3.1	Bending
S7	214.0	3.0	269.3	5.0	383.0	28.6	3.7	3.6	Bending
S8	218.5	2.9	307.4	5.0	415.2	24.4	2.6	2.6	Bending
S9	198.2	4.1	252.5	6.3	333.0	31.3	4.1	4.1	Bending
S10	175.9	5.2	195.6	6.2	246.9	44.5	4.8	4.9	Debonding, shear

Based on Figure 9 and Table 6, it can be seen that the bending load-deflection characteristics of steel-UHPC composite beams can be divided into 3 stages as observed in other investigations [13-14] and described below.

### 1) Elastic phase (0-A)

This phase spans from the initial loading to the cracking of the bottom flange of the concrete slab.. The relative slip between concrete and steel beams is relatively small, and the load-deflection curve is linear. At this stage, the composite beam exhibits a good composite action.

### 2) Nonlinear development phase (A-B)

As the load increased, the yield point of the bottom flange of the steel beam was gradually reached. Because of the nonlinear behavior of concrete in compression, the load-deflection curve exhibits a nonlinear characteristic, resulting in degradation of flexural stiffness. Vertical cracks continuously developed at the bottom of the mid-span concrete in specimens S1-S9, and expanded upward.

### 3) Hardening phase (B-C/D)

As the composite beam reached its yield point, the plastic strain at the bottom of the steel beam continued to increase, causing the steel to exhibit hardening behavior. With the load slowly increasing,

the deflections and interface slips significantly increased, resulting in a further degradation of flexural stiffness.

Generally, two types of load-deflection trend beyond point B were observed. Type I (B-D) behavior was exhibited by test specimen S10, where the adhesive layer failed prematurely, leading to delamination. As a result, the concrete slab and steel beam resisted the load independently, and the load-deflection curve showed obvious yielding. The concrete slab at the loading point experienced vertical cracks which extended throughout its depth, resulting in a decrease in beam stiffness and an increase in deflection. However, there was hardly any increase in the load (B-D). When the vertical cracks gradually penetrate throughout the concrete slab depth, the composite beam reached its ultimate load, and the load-deflection curve is of Type I.

On the other hand, Type II (B-C) was exhibited by specimens S1~S9 due to the effective composite action between concrete slab and steel beams as a result of the use of shear keys (SSK or bolts). Although the composite beam experienced reduction in stiffness, the load increases nonlinearly with the increase of deflection. The composite beam reached the ultimate load owing to the crushing of the upper concrete, and the load-deflection curve is of type II. According to the Chinese code [33], the deflection of the normal service state is defined as the mid-span deflection limit ( $\delta_{\text{limit}} = 6 \text{ mm}$ ), which equals 1/300 of the total span. The ultimate deflection of all specimens exceeded the deflection limit, which indicates that the designed steel-UHPC composite beam with SSK is capable to meet the limit state requirements for normal service.

#### 4.2.2 Deflection distribution along the span of specimens

Figure 10 shows the deflection distribution along the longitudinal direction of specimens. The deflection distribution of specimens S1-S9 appears to follow a half-cosine wave. Generally, for lower loads ( $P \leq 0.8 P_u$ ), the composite beams, overall, exhibited small deflection. However, when  $P = P_u$ , the composite beam deflections significantly increased, due to yielding of steel section. Even for specimens S2 and S3 having concrete strengths of C40 and C50, respectively with small ultimate deflections, the deflections are characterized by global rather than local deformations. This also confirms that specimens S1~S9 fail due to flexure. When  $P \leq 0.8 P_u$ , specimen S10 exhibited a symmetrical deflection. Nevertheless, when  $P = P_u$ , the concrete suffered shear interface failure as a result of the premature delamination along combined interface. The deflection in the damaged area (i.e. the loaded area where the through-crack occurs) is significantly greater than that on the other side.

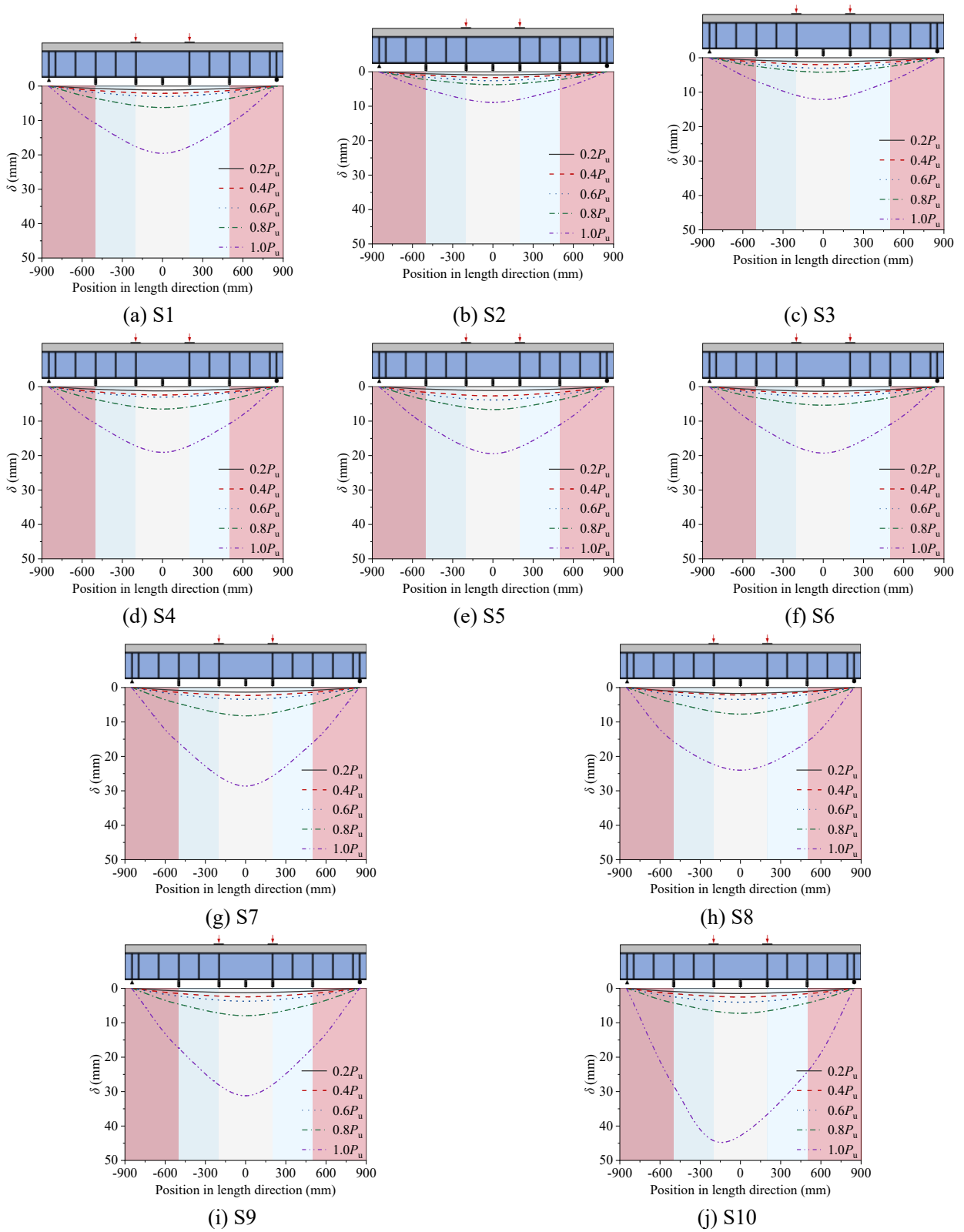


Fig. 10 Deflection distribution along the span of specimens

### 4.3 Load-strain response

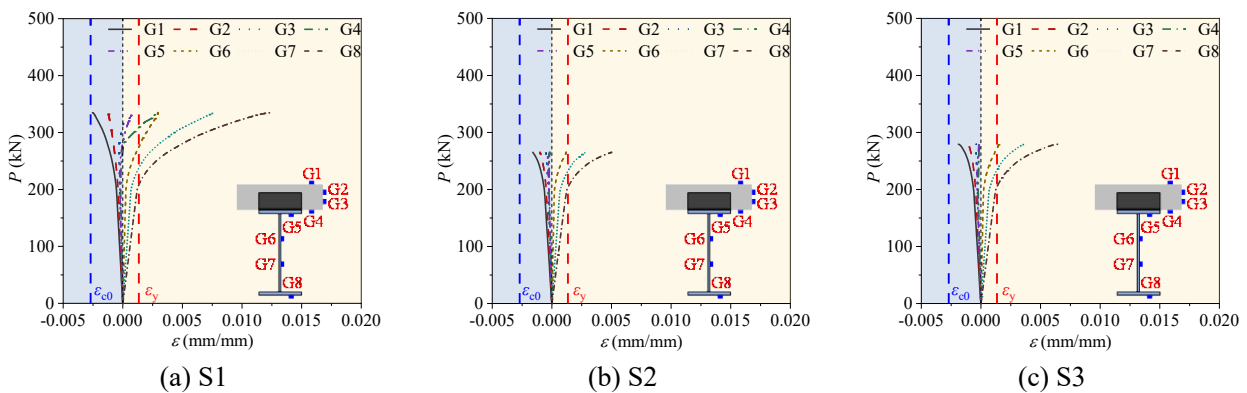
#### 4.3.1 Load-strain curves for major points at mid-span

Figure 11 shows the load-strain curves of the main measuring points at the mid-span cross-section, where,  $\varepsilon_{c0}$  is the peak compression strain of concrete (upper flange of concrete slab), and  $\varepsilon_y$

is the yield strain of steel beam (bottom flange of steel beam). When the specimens were in the elastic stage, the strain is linearly distributed, illustrating a good connection between concrete slabs and steel beam. During the nonlinear stage, the concrete and steel beam suffered greater strains, resulting in a gradual yielding of the lower flange and web of the section steel. When subjected to the same load during the hardening stage, the concrete experiences significantly less compressive strain than the steel.

It can be seen from Fig. 11a, 11d to 11j that the strains of G3 and G4 (strains in concrete) and G5 (strain in steel) are negative during the elastic stage. During the nonlinear development stage, it gradually changes from negative to positive, whereas during the hardening stage, it keeps positive. With the increase of load, the neutral axis moves from the steel web into the concrete slab. On the other hand, the strains of G1, G2, G3 (strains in concrete) and G5 (strain in steel) of specimens S2 and S3 remain positive, while the values of G6, G7, and G8 (strain in steel) also remain positive, suggesting that the neutral axis of specimens S2 and S3 consistently remained positioned at the steel web during the entire bending process. Thus, compared to NSC, UHPC can significantly improve bending stiffness of composite beams, utilize the tensile performance of section steel, and enhance material utilization efficiency.

As shown by specimen S10, the strain gauges G1, G2 (strain in concrete) and G5, G6 (strain in steel) stayed negative during the bending process. G1, which represents strain in concrete, is far from reaching its peak strain, while G3, G4 (strains in concrete) and G7, G8 (strains in steel) remain positive. Due to the destruction of the adhesive layer between the steel and concrete, the interface delamination occurs prematurely, and the concrete and steel work independently. Thus, welding shear keys (bolts and angle steel) are more effective than epoxy resin in enhancing the interface connection and improving the flexural performance of composite beams.



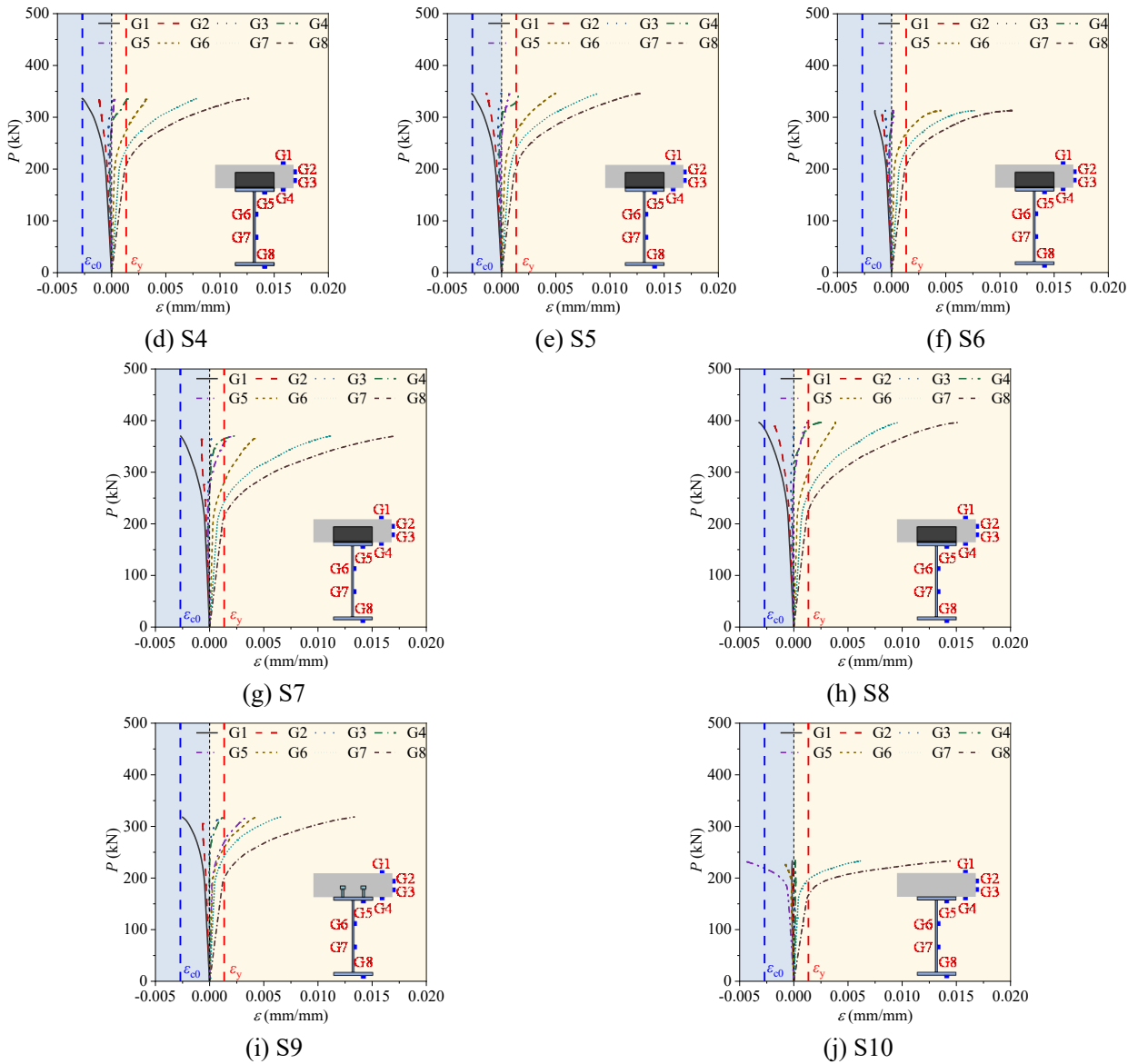


Fig. 11 Load-strain curves for major points at mid-span region

#### 4.3.2 Strain distribution along the height of cross section at mid-span

Figure 12 shows the strain distribution along the height at the mid-span section of composite beams. As can be seen from the figures, the strain distribution along the cross-section height of specimens S1~S9 is almost linear when  $P \leq 0.8P_u$ . The strain in concrete slab at the combined interface is approximately equal to the strain in the upper flange of section steel, and the strain distribution at mid-span section conforms to the plane section assumption. Due to the redistribution of stresses caused by the interfacial slip, the cross-section concrete strain along the height direction shows nonlinear distribution when  $P = P_u$ , illustrating that the mid-span section is no longer conforms to plane section assumption, but the curvature of the concrete slab and section steel is almost the same. The welded shear keys prevent the development of longitudinal bonding cracks parallel to steel flanges. It is evident that the UHPC is well connected and works well with the steel beam, confirming the efficiency of steel-UHPC composite beam with SSK. For specimen S10, as delamination between

concrete slab and steel beam took place at early stages of loading, the compressive strain of the concrete slab at the mid-span is relatively small.

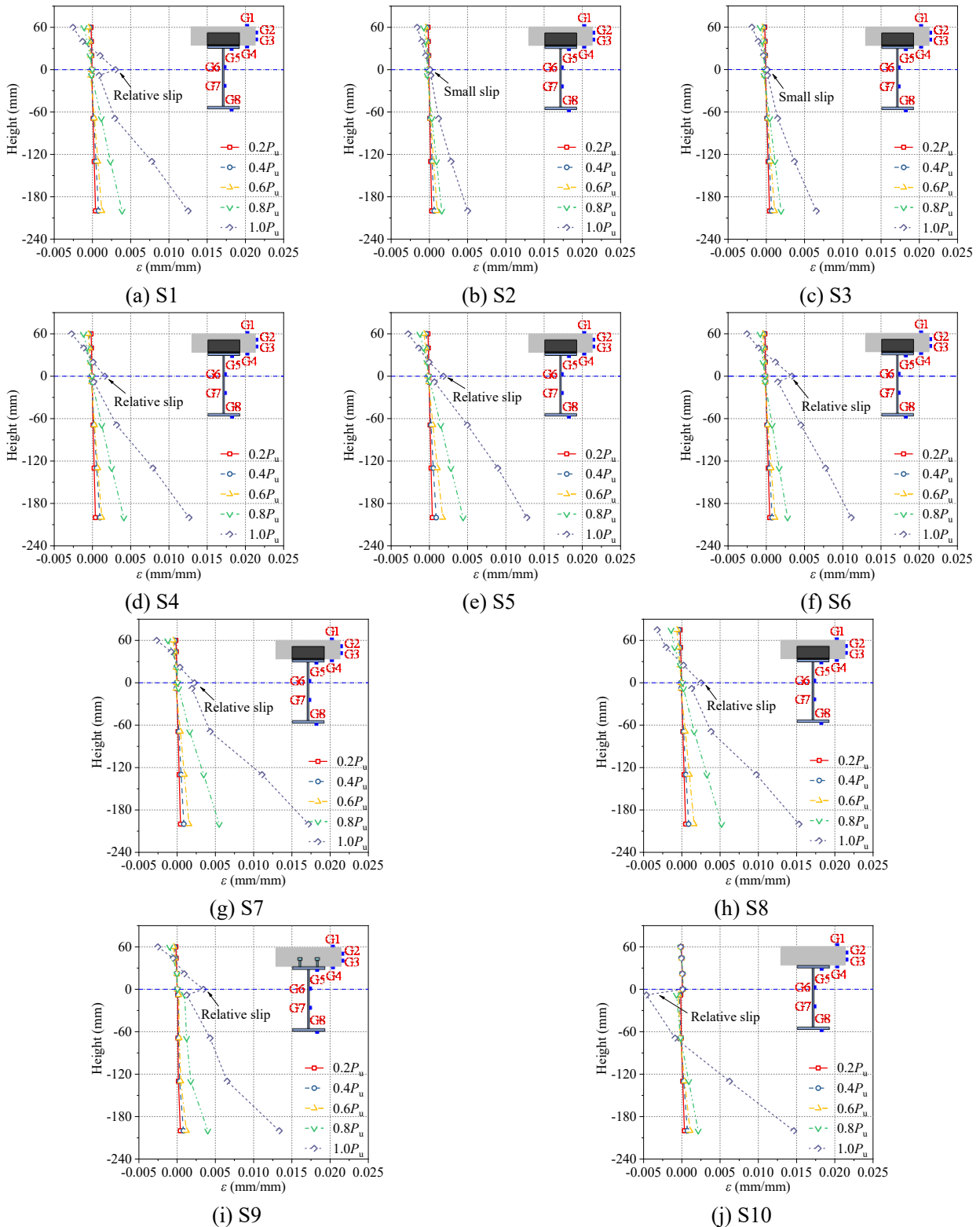
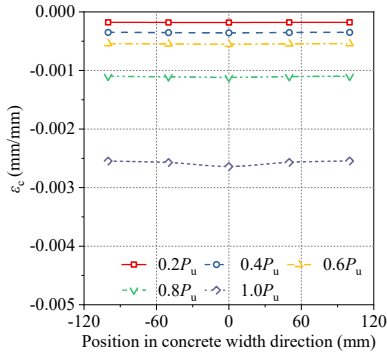


Fig. 12 Strain distribution along the height direction of cross section at mid-span

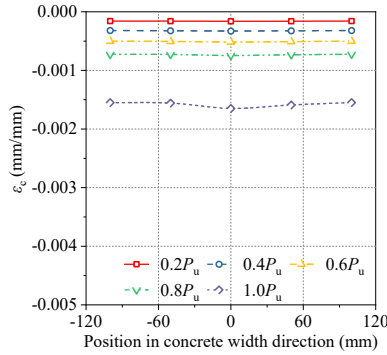
#### 4.3.3 Strain distribution at the top of concrete slab

Figure 13 illustrates the longitudinal strain distribution at the top of concrete slab. As can be seen in the figure, when  $P \leq 0.8P_u$ , the longitudinal strain of the concrete slab is evenly distributed. When

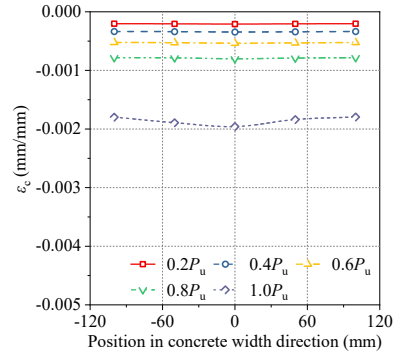
$P = P_u$ , the strain distribution exhibited a characteristic of "small at both ends and large in the middle". Concrete in the center region bears greater compressive stresses than those in the edge region, indicating the shear hysteresis effect [34]. Since the compressive stress acting on the concrete slab in the middle of the section is transmitted to the steel beam below, and the edge of the concrete plate is primarily used as a cantilever to distribute the external force. It is evident that specimen S7 exhibited a greater degree of shear hysteresis effect than other specimens. With the increase of the width of concrete slab, the shear hysteresis effect of the T-shaped composite beam becomes more evident.



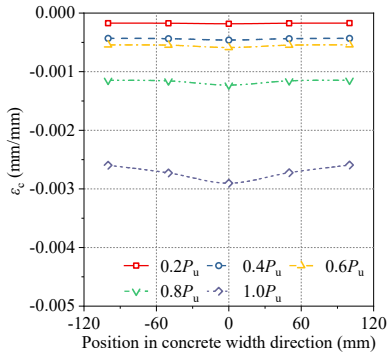
(a) S1



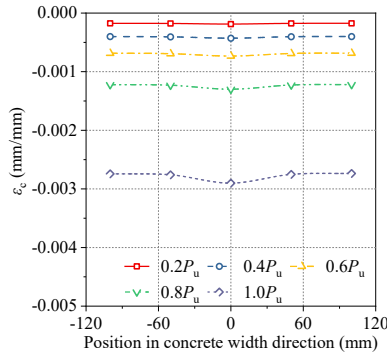
(b) S2



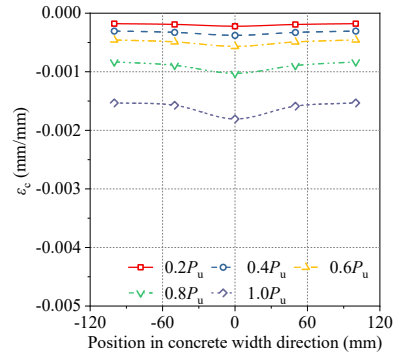
(c) S3



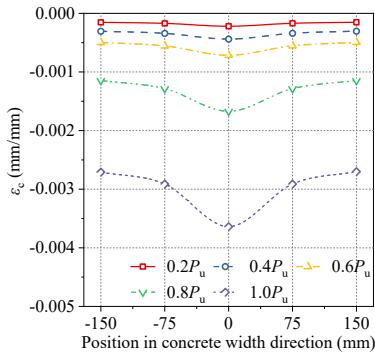
(d) S4



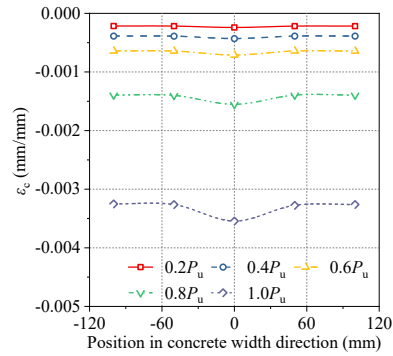
(e) S5



(f) S6



(g) S7



(h) S8

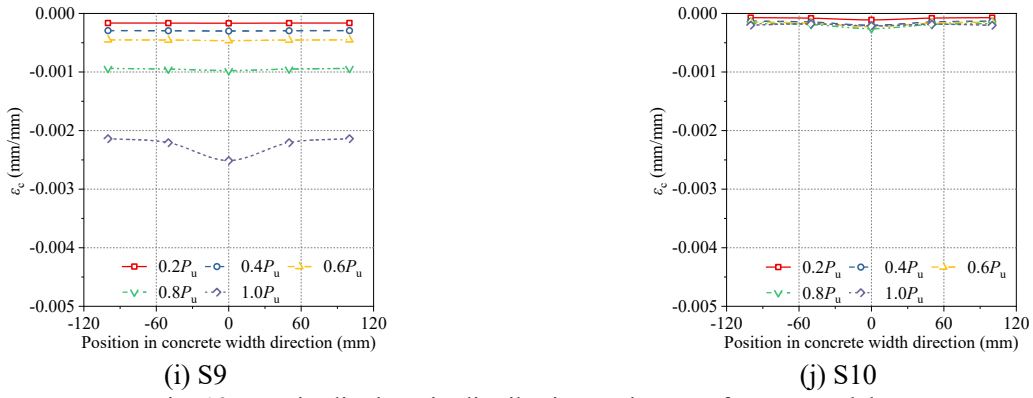


Fig. 13 Longitudinal strain distribution at the top of concrete slab

## 4.4 Load-slip response

### 4.4.1 Load-end slip curve

Figure 14 illustrates the load-end slip curves for all specimens. It can be seen from Figs. 9 and 14 that the load-end slip curves follow a similar pattern as the load-deflection curves in all three stages. During the elastic stage, the end slip is extremely small and increases linearly. During the nonlinear development stage, the end slip increases nonlinearly, and the increasing rate gradually increases. During the hardening stage, the end slip increases rapidly.

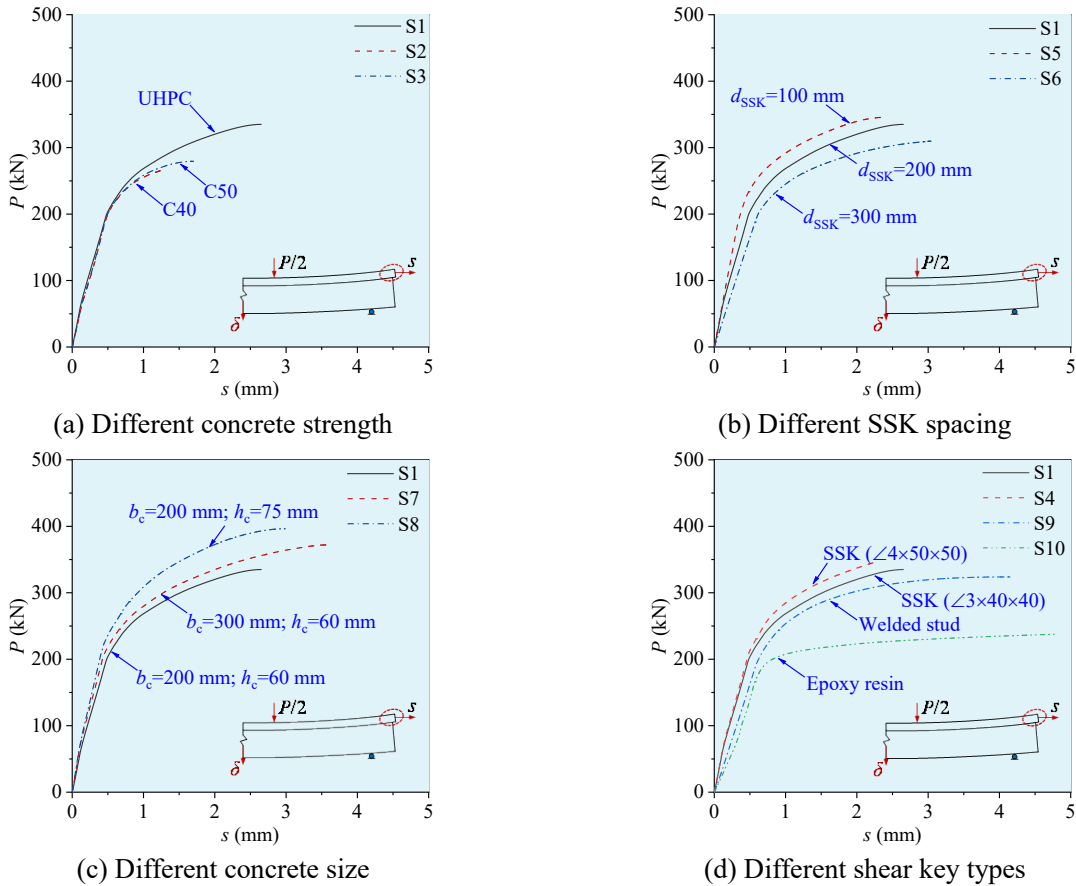


Fig. 14 Load-end slip curves

During the elastic stage, concrete strength has little effect on the end slip, and the composite interfaces of specimens S1, S2, and S3 have almost the same shear stiffness. During the nonlinear

development stage, the end slip of the composite beam increases with the increase of concrete strength, and the composite beam with UHPC slab exhibits a greater end slip than the composite beam with NSC slab.

The end slip of the composite beam having SSK with spacing of 100 mm is the smallest, and the shear stiffness is the highest; the end slip of the composite beam having SSK with spacing of 300 mm is the largest, and the shear stiffness is the lowest; and those of composite beam having SSK with spacing of 200 mm are in-between. It is evident that with the reduction of SSK spacing, the shear performance of the combined interface gradually improves, consequently enhancing the collaborative deformation capacity of composite beams and the overall bearing capacity, consistent with the test results of Zhang et al. [35].

The end slip of specimen with concrete slab of  $75 \times 200$  mm (height  $\times$  width) is greater than that of specimen with concrete slab of  $60 \times 200$  mm, but smaller than that of specimen with concrete slab of  $60 \times 300$  mm. However, the specimen with concrete slab of  $75 \times 200$  mm shows the greatest shear stiffness, the specimen with concrete slab of  $60 \times 200$  mm shows the lowest shear stiffness, the specimen with concrete slab of  $60 \times 300$  mm is in-between. Accordingly, increasing the area of concrete slab can effectively improve the shear stiffness of composite interface and bearing capacity of composite beam.

The epoxy-treated specimen exhibits the greatest end slip and the lowest interfacial shear stiffness. The specimen with welded SSK has smaller end slip and greater interfacial shear stiffness than the specimen with welded bolts. It indicates that the welded SSKs provide better interfacial shear resistance than welded bolts, as well as improving the bending resistance and cooperative deformation ability of composite beams. The specimen having SSKs with size of  $4 \times 50 \times 50$  mm has a smaller end slip and a greater interfacial shear stiffness than specimen having SSKs with size of  $3 \times 40 \times 40$  mm. With the increase of the size of SSK, the contact surface between the SSKs and concrete or upper flange of steel becomes larger, and the connection performance improves.

#### 4.4.2 Horizontal interfacial slip distributions along the beam length

Figure 15 shows the horizontal interfacial slip distributions along the beam length for all specimens. From Figs. 10 and 15, it can be seen that the deflection and relative slip of specimens S1~S9 are extremely small before  $0.6P_u$ , gradually increased from  $0.6P_u$  to  $0.8P_u$ , and significantly increased from  $0.8P_u$  to  $1.0P_u$ . Clearly, composite beams exhibit a good overall performance during the elastic stage. In addition, the relative slip gradually increases from the midspan to both ends, with an almost sinusoidal distribution curve along the beam length [36]. The maximum relative slip of the specimens with welded SSK is less than 4 mm, whereas the maximum relative slip of the specimens

with welded bolts is greater than 4 mm. The results demonstrate that welded SSK improves interface shear performance and composite action of beams more effectively than welded bolts. Since specimen S10 displays premature interface delamination, the midspan bending effect of concrete is minimal. The relative slip of specimen S10 is mainly distributed in the shear span section, while relative slip in the bending-shear section is very small.

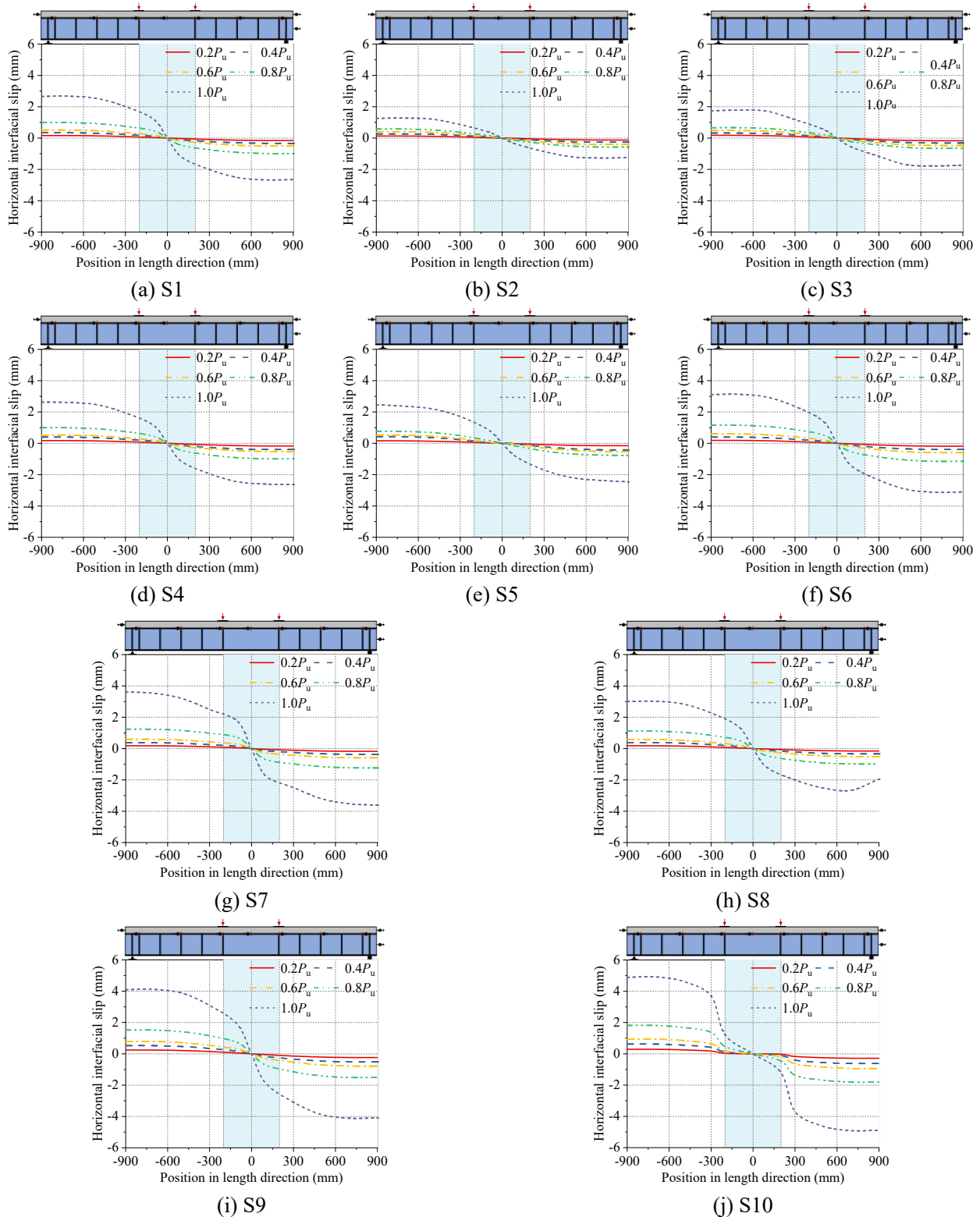


Fig. 15 Horizontal interfacial slip distributions along the beam length

## 4.5 Discussion of designed parameters

The effect of design parameters, such as strength of concrete, spacing of SSK, size of concrete slab and types of shear keys, on flexural performance of steel-UHPC composite beams are analyzed in this section. The cracking, yield and ultimate loads ( $P_{cr}$ ,  $P_y$  and  $P_u$ ) and corresponding deflections ( $\delta_{cr}$ ,  $\delta_y$  and  $\delta_u$ ), cracking, yield and ultimate stiffnesses ( $K_{cr}$ ,  $K_y$  and  $K_u$ , as presented in Eq. 1), ultimate energy dissipation ( $E_u$ ) and ductility ( $\mu$ , as shown in Eq. 2) are compared.

$$K_{cr} = \frac{P_{cr}}{\delta_{cr}} \quad (1-1)$$

$$K_y = \frac{P_y - P_{cr}}{\delta_y - \delta_{cr}} \quad (1-2)$$

$$K_u = \frac{P_u - P_y}{\delta_u - \delta_y} \quad (1-3)$$

$$\mu = \frac{\delta_u}{\delta_y} \quad (2)$$

### 4.5.1 Effect of concrete strength

Figure 16 illustrates the effect of concrete strength on flexural performance of composite beams. With the increase of concrete strength, the cracking, yield and ultimate loads, as well as the corresponding deflection of the composite beam, significantly increase. The ultimate load and deflection of UHPC composite beams are 28.8% and 124.1%, respectively, higher than those of specimen with C40, and 19.8% and 62.5%, respectively, higher than those of specimen with C50. With the increase of concrete strength, the compression zone of specimen with high strength concrete withstands greater pressure when compared with that of specimen with low strength concrete. At failure state, the tensile strain in the bottom flange of specimen with UHPC is greater than that of the specimen with NSC, leading to greater ultimate section curvature and deformation [37].

During the elastic stage, specimen with C40 has the lowest cracking stiffness  $K_{cr}$ , specimen with UHPC has the highest, and specimen with C50 is in-between. The "bridging effect" between the fibers and matrix causes UHPC to have a stronger tensile strength than NSC, delaying UHPC concrete slab cracking [38] and enhancing the cracking load of composite beams. During the nonlinear development stage and hardening stage, the yield stiffness  $K_y$  and ultimate stiffness  $K_u$  of specimen with C40 are the smallest, those of specimen with UHPC are the largest, and those of specimen with C50 are in-between. Because the yield and ultimate deflection of specimen with NSC are less than

those of specimen with UHPC, the composite beams with lower concrete strength crushed earlier. Consequently, the degradation of flexural stiffness is not obvious, and composite beam still has significant reserve of flexural strength.

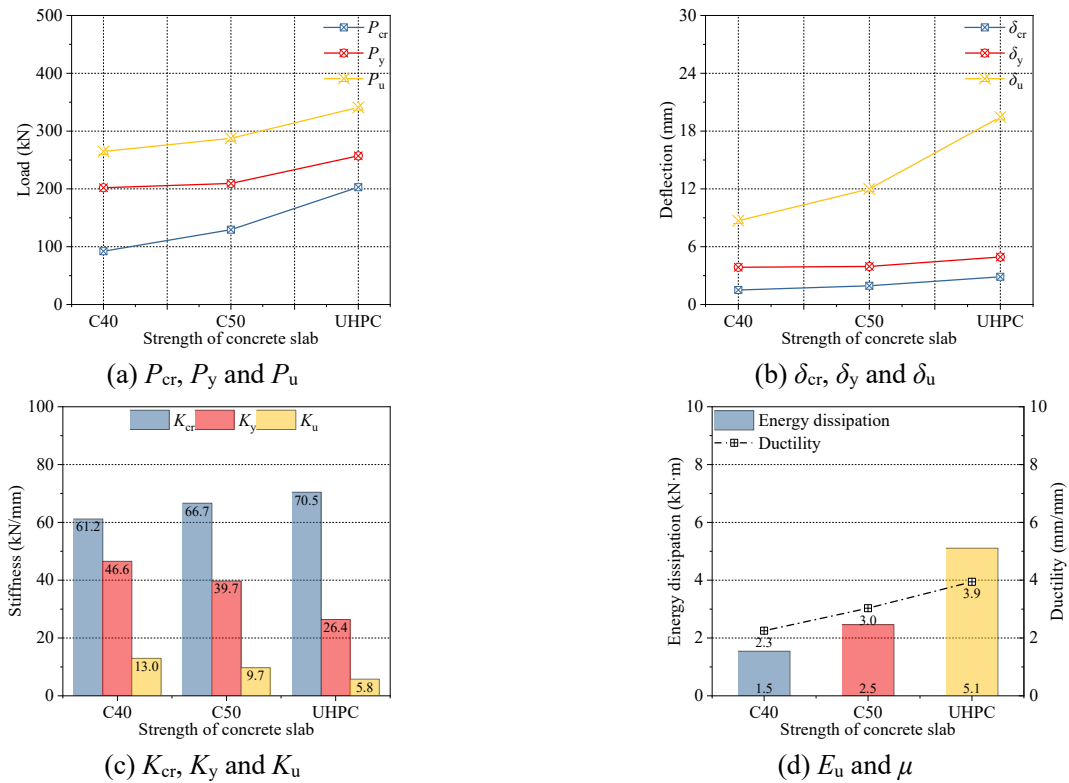


Fig. 16 Effects of concrete strength on flexural performance

#### 4.5.2 Effect of SSK spacing

Figure 17 illustrates the effect of SSK spacing on flexural performance of composite beams. With the increase of SSK spacing, the characteristic loads ( $P_{cr}$ ,  $P_y$  and  $P_u$ ) of the composite beam gradually decrease, while the characteristic deflections ( $\delta_{cr}$ ,  $\delta_y$  and  $\delta_u$ ) increase, indicating that the smaller the SSK spacing, the better the interface bond between concrete and steel, and bearing capacity improves accordingly. As the spacing between SSK decreases, the flexural stiffness ( $K_{cr}$ ,  $K_y$  and  $K_u$ ) also increases, while the corresponding deflection decreases. The ductility of specimen with SSK spacing of 300 mm is 25.6% and 32.4%, respectively, higher than that of the specimen with SSK spacing of 200 and 100 mm, and the ultimate energy dissipation increases by 15.6% and 22.9%, respectively, indicating that the specimen with SSK spacing of 300 mm have the most superior ductility and energy dissipation capabilities.

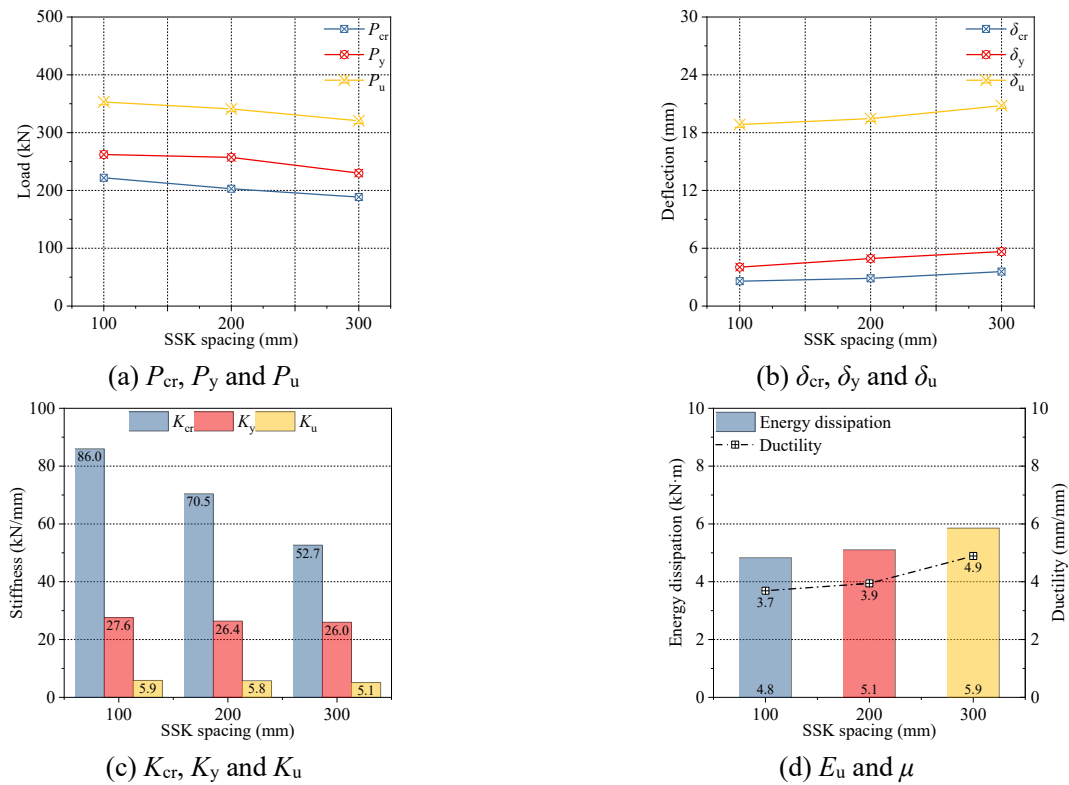


Fig. 17 Effects of SSK spacing on flexural performance

#### 4.5.3 Size effect of concrete slab

Figure 18 illustrates the size effect of concrete slab on flexural performance of composite beams. With the increase of height or width of concrete slab, the characteristic loads ( $P_{cr}$ ,  $P_y$  and  $P_u$ ) and corresponding deflections ( $\delta_{cr}$ ,  $\delta_y$  and  $\delta_u$ ), as well as ductility and ultimate energy dissipation of composite beams increase. With the increase of height or width of concrete slab, the moment of resistance resulted from concrete compression and steel beam tension increases (the value and arm of force increase simultaneously) and therefore, the moment capacity increases. The tensile strain at the bottom flange of specimen with large concrete slab is greater than that of specimen with small concrete slab, leading to a greater ultimate curvature and deformation.

The ultimate load and deflection of specimen having concrete slab with size of  $60 \times 300$  mm (height  $\times$  width) are greater than those of specimen having concrete slab with size of  $60 \times 200$  mm, respectively, while the ultimate load and deflection of specimen having concrete slab with size of  $75 \times 200$  mm are greater than those of specimen having concrete slab with size of  $60 \times 200$  mm by 21.7% and 25.1%. Accordingly, the height of concrete slab has a greater effect on bending capacity and flexural stiffness ( $K_{cr}$ ,  $K_y$  and  $K_u$ ) of composite beams, whereas the width of concrete slab has a greater effect on ultimate deflection, ductility and energy dissipation. Therefore, specific design of concrete slab cross-section can be used in engineering applications to achieve different structural performance.

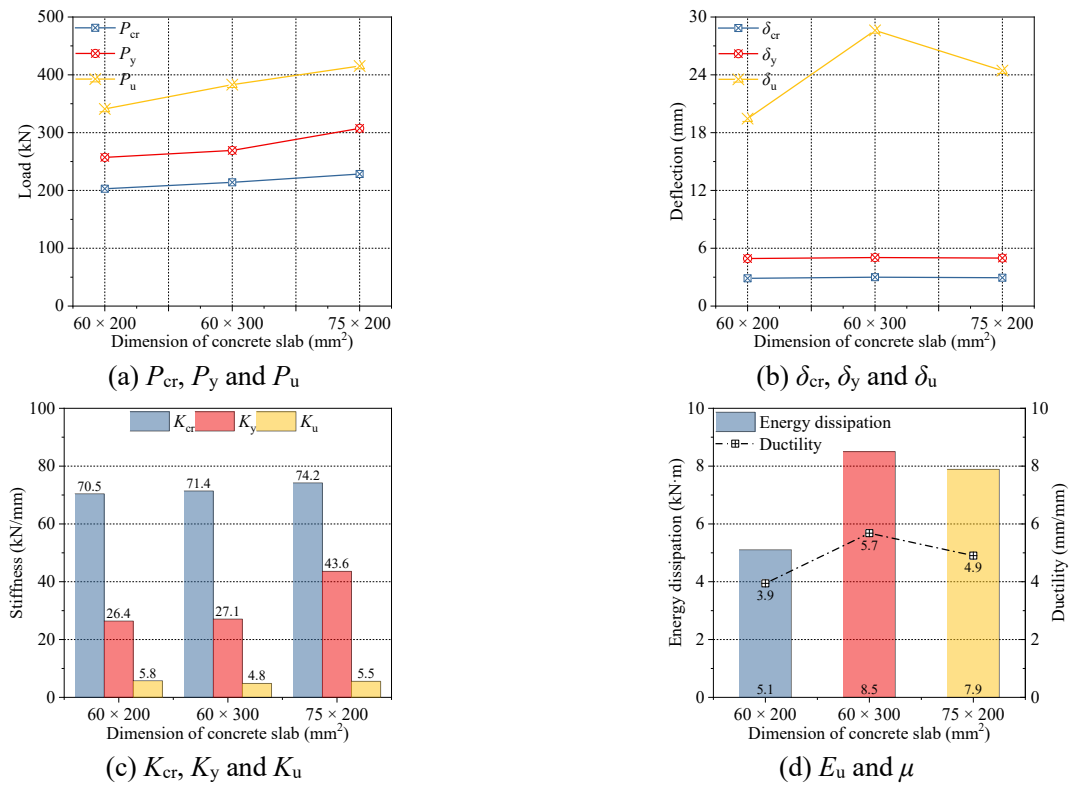


Fig. 18 Effects of concrete slab size on flexural performance

#### 4.5.4 Effect of SSK types

Figure 19 illustrates the effect of SSK type on flexural performance of composite beam. As observed that the specimen with large size of SSK has higher characteristic loads ( $P_{cr}$ ,  $P_y$  and  $P_u$ ), flexural stiffness ( $K_{cr}$ ,  $K_y$  and  $K_u$ ), and ultimate energy dissipation, but smaller characteristic deflections ( $\delta_{cr}$ ,  $\delta_y$  and  $\delta_u$ ) and ductility than the specimen with small size of SSK. It is evident that the large-size SSK has stronger interface connection, significantly promoting the interfacial shear resistance of composite beam and overall composite action.

When examining the specimens with small size of SSK, welded bolts and epoxy resin, it becomes apparent that the composite beam with SSK has the largest characteristic loads ( $P_{cr}$ ,  $P_y$  and  $P_u$ ) and flexural stiffness ( $K_{cr}$ ,  $K_y$  and  $K_u$ ). On the other hand, the epoxy-treated specimen have the smallest characteristic loads and flexural stiffness, while that with welded bolts fall somewhere in between. However, the characteristic deflections ( $\delta_{cr}$ ,  $\delta_y$  and  $\delta_u$ ) and ductility display an opposite trend. Thus, specimen with welded SSK exhibits superior interfacial shear performance and is the most effective in improving flexural capacity and stiffness of steel-UHPC composite beams when compared to counterparts with other types of shear connectors.

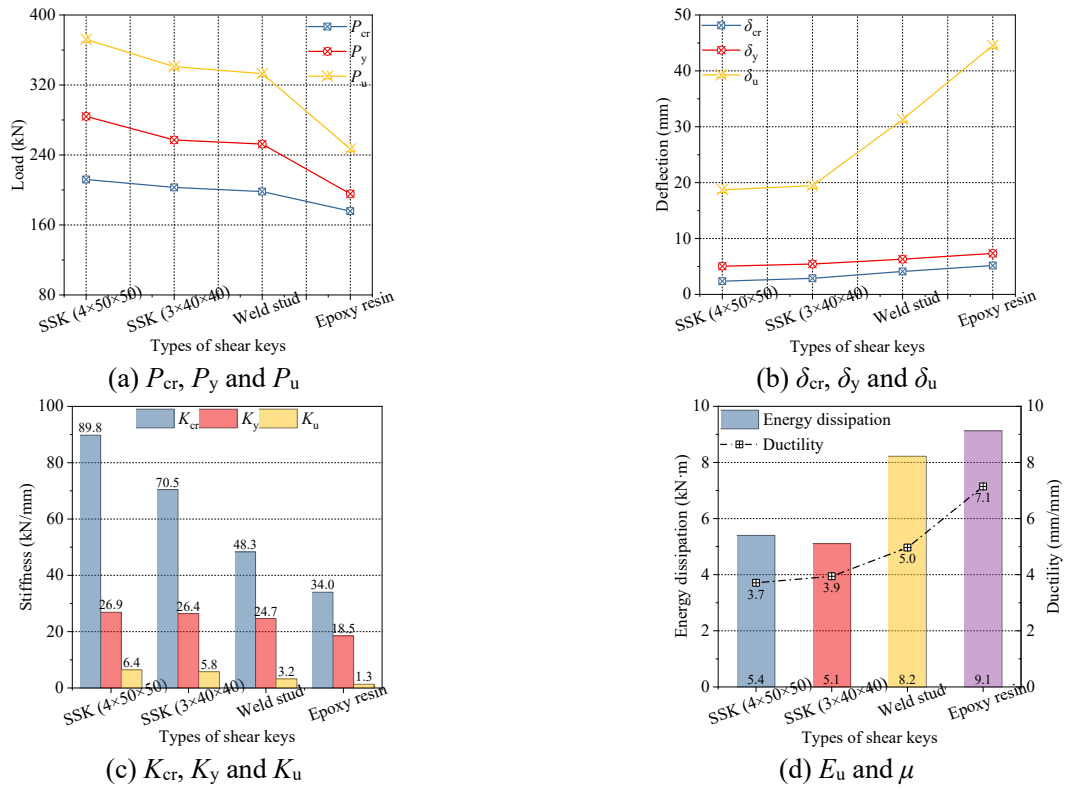


Fig. 19 Effects of shear keys' types on flexural performance

## 5 Flexural capacity prediction of steel-UHPC composite beams

### 5.1 Failure mode and boundary failure

The failure modes of all specimens can be classified into four types (A, B, C, and D). Below are further descriptions of these modes of failure, where,  $\varepsilon_c$ ,  $\varepsilon_s$  and  $\tau$  are the compressive strain of UHPC, tensile strain of steel beam and horizontal shear stress, respectively;  $\varepsilon_{cu}$ ,  $\varepsilon_{sy}$  and  $\varepsilon_{su}$  are the ultimate compressive strain of UHPC, yield and ultimate tensile strain of steel beam, respectively;  $\tau_u$  are the ultimate horizontal shear stress.

1) Failure mode A:  $\varepsilon_c = \varepsilon_{cu}$ ,  $\varepsilon_s < \varepsilon_{sy}$ . The compression UHPC reaches its ultimate compressive strain, but the maximum tensile strain of section steel has not yielded. This failure mode is similar to the failure mode of over-reinforced RC beams, and is not recommended in practice due to its brittleness.

2) Failure mode B:  $\varepsilon_c = \varepsilon_{cu}$ ,  $\varepsilon_{sy} < \varepsilon_s \leq \varepsilon_{su}$ . The compression UHPC reaches its ultimate compressive strain after the yielding of section steel; however, the maximum tensile strain of section steel is less than its ultimate strain. This failure mode is similar to the failure mode of under-reinforced RC beams, and is recommended in practical purposes due to its ductility and efficient utilization of materials strengths.

3) Failure mode C:  $\varepsilon_c < \varepsilon_{cu}$ ,  $\varepsilon_s = \varepsilon_{su}$ . The maximum tensile strain of section steel reaches its ultimate strain while the compressive UHPC does not attain the ultimate compressive strain. Namely,

the section steel fractures before the crushing of UHPC. This failure mode is brittle, hence not recommended in engineering structures.

4) Failure mode D:  $\varepsilon_c < \varepsilon_{cu}$ ,  $\tau = \tau_u$ . The horizontal shear stress of the composite interface reaches the ultimate shear stress, while the compressive UHPC does not attain the ultimate compressive strain. Specifically, the composite interface fails completely before UHPC crushing, resulting in concrete slab and steel section no longer functioning together as a composite section, leading to significant slip in the composite beam.

Based on the analysis of the three flexural failure modes (A, B, and C), it can be found that there are two boundary failures, as shown in Fig. 20, where,  $x_{c1}$  and  $x_{c2}$  are the height of compression zone at boundary failure states 1 and 2, respectively.

1) Boundary failure 1:  $\varepsilon_c = \varepsilon_{cu}$ ,  $\varepsilon_s = \varepsilon_{sy}$ ; that is crushing of UHPC and yielding of section steel occur simultaneously. Here, the height of compression zone  $x_{c1} = \varepsilon_{cu} / (\varepsilon_{cu} + \varepsilon_{sy}) h$ .

2) Boundary failure 2:  $\varepsilon_c = \varepsilon_{cu}$ ,  $\varepsilon_s = \varepsilon_{su}$ . The compression UHPC and maximum tensile strain in section steel reach their respective ultimate strain at the same time. That is the crushing of UHPC and fracture of section steel occur simultaneously. Here, the height of compression zone  $x_{c2} = \varepsilon_{cu} / (\varepsilon_{cu} + \varepsilon_{su}) h$ .

So, if the height of compression zone  $x_c > x_{c1}$ , failure mode A occurs; if  $x_{c2} \leq x_c \leq x_{c1}$ , failure mode B occurs; if  $x_c < x_{c2}$ , failure mode C occurs.

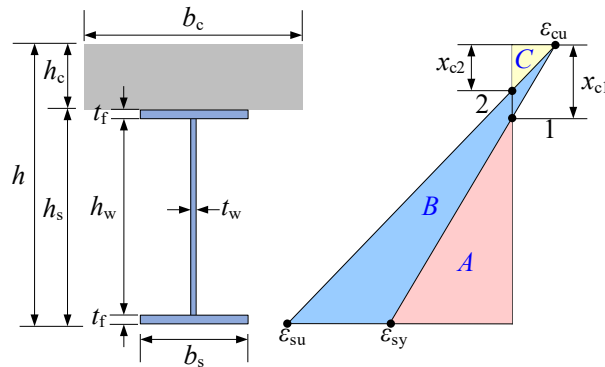


Fig. 20 Strain distribution of cross-section under two types of boundary failure

## 5.2 Calculation formula for flexural capacity

Based on the analysis of the failure modes and basic assumptions, the bearing capacity of composite beams is proposed. Here, the following assumptions have been considered. 1) No slip occurs between the steel beam and UHPC slab. 2) The strain in the cross-section consistent with the plane-section assumption. 3) The specimens considered to be failed when either the extreme tensile steel or compressive UHPC reaches their respective ultimate strain. As S10 exhibited signs of loss of bond between the steel beam and concrete flange and failed prematurely, it has not been taken into

account in this theoretical analysis.

### 5.2.1 Material constitutive models

Figure 21 shows the compressive stress-strain curves of NSC and UHPC. The compressive and tensile stress-strain curves of NSC are referred to the Chinese code GB 50010-2010) [26], which is not described here. The tensile strength  $f_t$ , compressive strength  $f_c$ , and elastic modulus  $E_c$  of NSC and UHPC are calculated obtained from the test results presented in Table 3. According to Zheng et al. [27], the compressive stress-strain constitutive relationship of UHPC can be expressed as follows:

$$y = \begin{cases} 1.55x - 1.2x^4 + 0.65x^5 & , 0 \leq x < 1 \\ x / [6(x-1)^2 + x] & , x \geq 1 \end{cases} \quad (3)$$

where  $x = \varepsilon_c / \varepsilon_{c0}$ ,  $y = \sigma_c / f_c$ ,  $\sigma_c$  and  $\varepsilon_c$  are the stress and the corresponding strain of concrete under compression.

Figure 22 shows the simplified tensile stress-strain curves of Q235 steel beam that is given below:

$$\sigma_s = \begin{cases} E_s \varepsilon_s & , 0 < \varepsilon_s \leq \varepsilon_y \\ f_y & , \varepsilon_s > \varepsilon_y \end{cases} \quad (4)$$

where  $\sigma_s$  and  $\varepsilon_s$  are the tensile stress and the corresponding strain of steel beam, respectively;  $f_y$  and  $\varepsilon_y$  are the yield stress and corresponding strain, respectively.

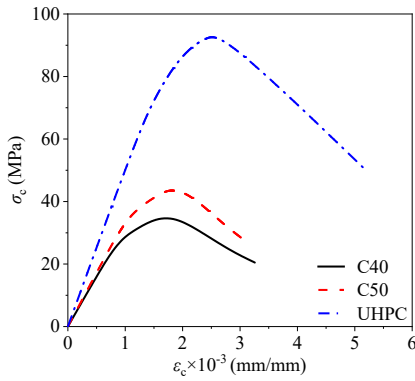


Fig. 21 Compressive stress-strain curves of concrete

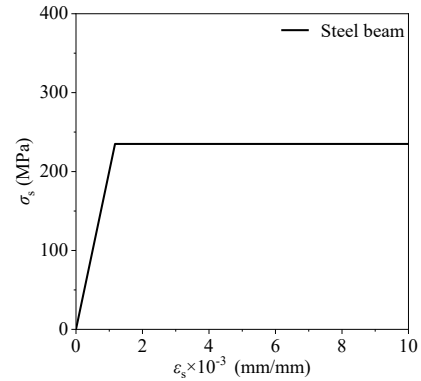


Fig. 22 Tensile stress-strain curve of steel beam

The calculation of section forces for equilibrium consideration depends on the location of the neutral axis, namely inside or outside the UHPC slab. Therefore, there are two cases to be analysed as explained below.

### 5.2.2 Section type I ( $x_c \leq h_c$ )

This case occurs when the height of compression zone  $x_c$  is smaller than that of UHPC slab,  $h_c$ ,

that is the neutral axis is in the UHPC slab. The cross-section strain and simplified stress distributions are shown in Fig. 23.

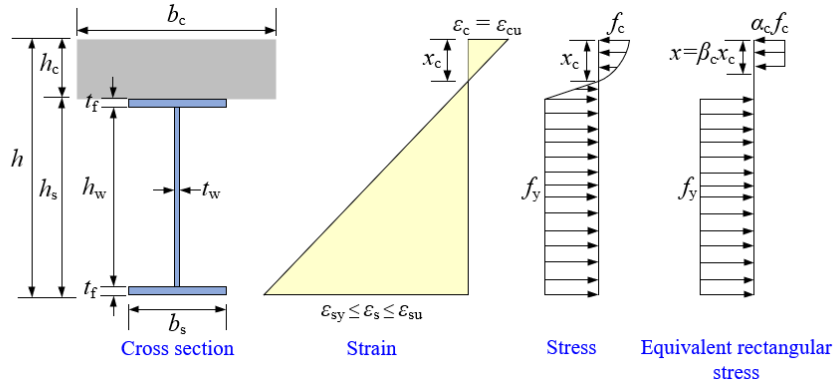


Fig. 23 Cross section strain and simplified stress distributions of type I

Equation (5) can be obtained according to the force equilibrium of cross-section, where  $A_s$  is the area of I-steel;  $x$  is the height of the equivalent compressive UHPC zone,  $x = \beta_c x_c$ ;  $\alpha_c$  and  $\beta_c$  are coefficients related to the mechanical properties of UHPC, which may be taken as 0.885 and 0.75 [39-40], respectively. And it is assumed that the lower flange and web of section steel are all yielded, and the tension of upper flange is neglected.

$$\alpha_c f_c b_c x = f_y A_s \quad (5)$$

Solving for  $x$ , Eq. (6) can be obtained.

$$x = \frac{f_y A_s}{\alpha_c b_c f_c} \quad (6)$$

As the height of compression zone should be smaller than the height of UHPC slab ( $x_c \leq h_c$ ) and  $x = \beta_c x_c$ , so, the obtained  $x$  should be less than  $\beta_c h_c$ , that is  $x \leq \beta_c h_c$ . Taking the resultant point of UHPC compression zone as inertia axis, the moment capacity  $M_u$  can be obtained as below.

$$M_u = f_y A_s \left( h - \frac{h_s}{2} - \frac{x}{2} \right) \quad (7)$$

### 5.2.3 Section type II ( $x_c > h_c$ )

When the height of the compression zone  $x_c$  exceeds the height of UHPC slab  $h_c$ , leading to the neutral axis being located in the section steel, the specimen experiences section type II failure mode. The cross-section strain and simplified stress distributions are shown in Fig. 24.

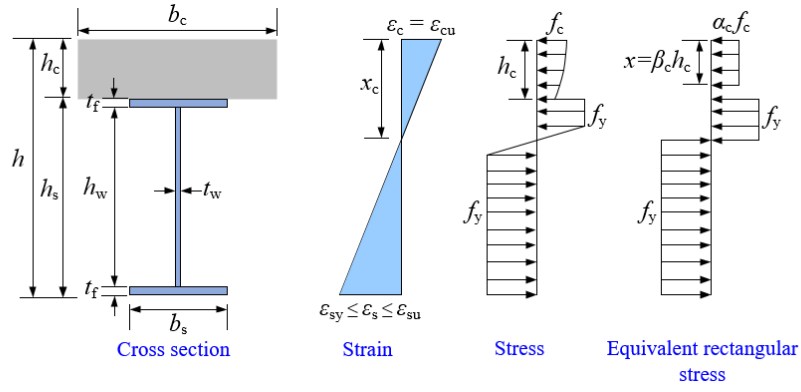


Fig. 24 Cross section strain and simplified stress distributions of type II

Equation (8) can be obtained by utilizing the force equilibrium of cross-section, where the upper flange under compression and bottom flange under tension, web of section steel under compression and tension are all assumed to be yielded.

$$\alpha_c b_c f_c h_c + f_y [b_s t_w + t_w (x - h_c - t_f)] = f_y [b_s t_w + t_w (h - x - t_f)] \quad (8)$$

Solving for  $x$ , Eq. (9) can be obtained.

$$x = \frac{1}{2} \left( h + h_c - \frac{\alpha_c b_c f_c h_c}{f_y t_w} \right) \quad (9)$$

Taking the resultant point of steel beam tensile zone as inertia axis, the moment capacity  $M_u$  can be obtained as below.

$$M_u = \alpha_c f_c b_c h_c \left( h - \frac{h-x}{2} - \frac{h_c}{2} \right) + f_y b_s t_f \left( h - \frac{h-x}{2} - h_c - \frac{t_f}{2} \right) + f_y t_w (x - h_c - t_f) \left( \frac{h - h_c - t_f}{2} \right) \quad (10)$$

### 5.3 Comparisons between experimental and theoretical capacities of composite beams

Figure 25 shows the comparison between the experimental and predicted values of ultimate load, and Table 7 summarizes the tested and calculated results, where  $P_{u,exp}$  and  $P_{u,cal}$  are the tested and calculated ultimate loads, respectively. All specimens except S10 occur section type I failure mode, which are consistent with the experimental results. The experimental failure load of S10 is expected to be far much less than the prediction from Eq. (7) or (9), as the interface bond between concrete slab flange and steel beam prematurely failed. The predicted failure loads of S1, S4, S5, S6 and S9 are the same as they had the same beam section and materials. Since the average and coefficient of variation, CoV, of  $P_{u,exp}/P_{u,cal}$  are 1.06 and 0.12, respectively, confirming the validity of the proposed formula to be used in the prediction of composite beams similar to those presented in this paper.

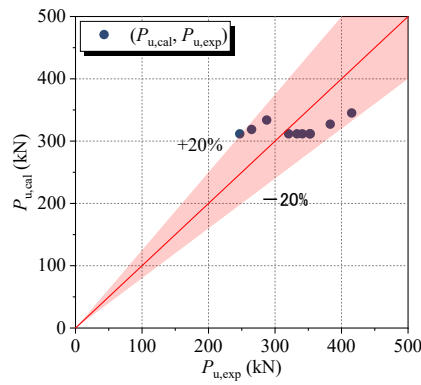


Fig. 25 Comparison between the tested and the calculated ultimate loads

Tab. 7 Summary of experimental and predicted values

No.	$P_{u,exp}$ (kN)	$P_{u,cal}$ (kN)	Section type	$P_{u,exp} / P_{u,cal}$
S1	341.0	311.7	I	1.09
S2	264.8	318.8	I	0.83
S3	287.5	333.9	I	0.86
S4	352.2	311.7	I	1.13
S5	353.0	311.7	I	1.13
S6	320.5	311.7	I	1.03
S7	383.0	327.3	I	1.17
S8	415.2	345.3	I	1.20
S9	333.0	311.7	I	1.07
Average				1.06
CoV				0.12

## 6 Conclusions

In this paper, a novel steel-UHPC composite beam with welded SSK is proposed and tested in four-point bending. Based on the research results, the following conclusions may be drawn.

1) All steel-UHPC composite beams with welded SSKs or welded bolts exhibited flexural failure, signified by slab concrete crushing and yielding of steel beam. However, composite beam treated with epoxy resin has failed due to the premature delamination of concrete slab and steel beam.

2) The strain distribution along the mid-span cross-section height of steel-UHPC composite beams with welded SSKs or welded bolts conforms to the plane section assumption before failure. However, close to the ultimate load, the strain distribution deviates from the plane section assumption because of the significant relative slip. For the composite beam treated with epoxy resin, the concrete slab and steel beam worked independently due to the premature delamination and therefore, compressive strain of mid-span concrete is extremely small, and the strain distribution along the full section never followed the plane section assumption. With the increase of width of concrete slab, the shear hysteresis effect of the T-shaped composite beam becomes more evident.

3) The end slip of composite beams increased with the increase of concrete strength, and the UHPC composite beam exhibited a greater amount of end slip than the composite beam with NSC. The ultimate load and deflection of composite beams with UHPC slab were 28.8% and 124.1%,

respectively, higher than those of specimen with C40 concrete slab, and 19.8% and 62.5%, respectively, higher than those of specimen with C50 concrete slab. With the increase of concrete strength, composite beams have an enhanced ductility and ability to dissipate energy.

4) Increasing the size of concrete slab can effectively improve the shear stiffness of composite interface. The height of concrete slab has a greater effect on bending capacity and flexural stiffness of composite beam, whereas the width of concrete slab has a greater effect on ultimate deflection, ductility and energy dissipation of composite beam. Therefore, specific design of cross-section can be used in engineering applications to achieve different structural properties.

5) With the decrease of SSK spacing, the shear performance of combined interface gradually improved. The cracking, yield, and ultimate load of composite beams gradually decreased with the increase of SSK spacing, while their corresponding displacement increased. The composite beam with SSK spacing of 300 mm exhibited the largest ductility and energy dissipation.

6) The effect of welding SSK is significantly greater than that of welding bolts when it comes to improving the interfacial shear performance and interoperability of composite beams, and the larger the size of SSK, the larger the effect. The welded SSK is most effective in improving the flexural capacity and stiffness of composite beams when compared to specimens with other types of shear keys. The large-size SSK has stronger capacity to promote the interfacial shear performance and overall working performance of composite beam.

7) Formulas for bearing capacity of steel-UHPC composite beams are developed based on simplified materials constitutive model and reasonable basic assumptions. The predicted results are in good agreement with the tested results, serving as a reference for the design and construction of steel-UHPC composite beams.

Compared to traditional steel-concrete composite beams, the steel-UHPC composite beams with welded SSK proposed in this study have superior structural performance (e.g. flexural capacity, interfacial shear performance, ductility and energy dissipation), thus tackling the challenge of large self-weight and high structure costs.

## **Credit authorship contribution statement**

**Zhiwen Zhang:** Investigation, Software, Formal analysis, Writing - Original draft, Review & Editing. **Ashraf Ashour:** Conceptualization, Methodology, Supervision, Writing - Review & Editing. **Wenjie Ge:** Formal analysis, Supervision, Writing - Review & Editing. **Zenghao Ni:** Formal analysis, Supervision, Review & Editing. **Hongbo Jiang:** Review & Editing. **Yan Liu:** Review & Editing.

## **Declaration of Competing Interest**

The authors declare that they have no known competing financial interests or personal relationships that could have appeared to influence the work reported in this paper.

## Acknowledgement

The authors would like to acknowledge the financial support to the work by the High-End Foreign Experts Project of Ministry of Science and Technology, China (G2022014054L), the Natural Science Foundation of Jiangsu Province, China (BK20201436), the Science and Technology Project of Jiangsu Construction System (2018ZD047, 2021ZD06), the Science and Technology Project of Gansu Construction System (JK2021-19), the Opening Foundation of Jiangsu Province Engineering Research Center of Prefabricated Building and Intelligent Construction, the Science and Technology Cooperation Fund Project of Yangzhou City and Yangzhou University (YZ2022194, YZU212105).

## Reference

- [1] J.G. NIE, Z.W. YU, Research and practice of composite steel-concrete beams in China, *China Civl. Eng. J.* 32 (4) (1999) 3-8. (in Chinese)
- [2] K.S. FAN, J.G. NIE, Progress in research and application of composite steel concrete bridges, *Prog. Steel Buil. Struct.* 8 (5) (2006) 35-39. (in Chinese)
- [3] E. Tan, B. Uy. Experimental study on straight composite beams subjected to combined flexure and torsion, *J. Constr. Steel Res.* 65 (2009) 784-793.
- [4] A. Souici, J.F. Berthet, A. Li, N. Rahal, Behaviour of both mechanically connected and bonded steel-concrete composite beams, *Eng. Struct.* 49 (2013) 11-23.
- [5] P. Richard, M. Cheyrezy. Composition of reactive powder concretes, *Cement Concrete Res.* 25 (7) (1995) 1501-1511.
- [6] P. Richard, M. Cheyrezy, Reactive powder concrete with high ductility and 200~800 MPa compressive strength, *ACI SP.* 144 (3) (1994) 507-518.
- [7] N.M. Azmee, N. Shafiq, Ultra-high performance concrete: From fundamental to applications, *Case Stu. Constr. Mat.* 9 (2018) e00197.
- [8] J. Du, W.N. Meng, K.H. Khayat, Y. Bao, P.W. Guo, Z.H. Lyu, A. Abu-obeidah, H. Nassif, H. Wang, New development of ultra-high-performance concrete (UHPC), *Compos. Part B-Eng.* 224 (2021) 109220.
- [9] W.L. Lu, W.Q. Peng, L. Zhu, B. Ma, F.L. Li, Study on mechanical behavior of steel-UHPC-NC composite beams under negative bending moment, *Case Stu. Constr. Mat.* 17 (2022) e01593.
- [10] X.D. Zhao, X.D. Shao, J.H. Cao, Z.X. Shao, R.J. Ying-Li, Experimental studies on shear behavior of steel-UHPC composite beam with hot rolled shape steel, *Eng. Struct.* 274 (2023) 115160.
- [11] J.S. Zhu, Y.G. Wang, J.B. Yan, X.Y. Guo, Shear behaviour of steel-UHPC composite beams in waffle bridge deck, *Compos. Struct.* 234 (2020) 111678.
- [12] J.S. Zhu, X.Y. Guo, J.F. Kang, M.H. Duan, Y.G. Wang, Numerical and theoretical research on flexural behavior of steel-UHPC composite beam with waffle-slab system, *J. Constr. Steel Res.* 171 (2020) 106141.
- [13] J.B. Yan, H.N. Guan, T. Wang, Steel-UHPC-steel sandwich composite beams with novel enhanced C-channel

- connectors: Tests and analysis, *J. Constr. Steel Res.* 170 (2020) 106077.
- [14] J.B. Yan, H.N. Guan, T. Wang, Numerical studies on steel-UHPC-steel sandwich beams with novel enhanced C-channels, *J. Constr. Steel Res.* 170 (2020) 106070.
- [15] B. Huh, C. Lam, B. Tharmabala, Effect of shear stud clusters in composite girder bridge design, *Can. J. Civl. Eng.* 42 (4) (2015) 150218143603005.
- [16] Y.B. Luo, K. Hoki, K. Hayashi, M. Nakashima, Behavior and Strength of Headed Stud-SFRCC Shear Connection. I: Experimental Study, *J. Struct. Eng.* 142 (2016) 4015112-1-4015112-10.
- [17] Y.B. Luo, K. Hoki, K. Hayashi, M. Nakashima, Behavior and Strength of Headed Stud-SFRCC Shear Connection. II: Strength Evaluation. *J. Struct. Eng.* 142 (2016) 04015113.1-04015113.10.
- [18] C. Xu, Q. Su, K. Sugiura, Mechanism study on the low cycle fatigue behavior of group studs shear connectors in steel-concrete composite bridges, *J. Constr. Steel Res.* 138 (2017) 196-207.
- [19] J.Q. Wang, Q.Z. Xu, Y. M. Yao, J.N. Qi, H.L. Xiu, Static Behavior of Grouped Large Headed Stud-UHPC Shear Connectors in Composite Structures, *Compos. Struct.* 206 (2018) 202-214.
- [20] Z.C. Fang, H.Z. Fang, P.J. Li, H.B. Jiang, G.F. Chen, Interfacial shear and flexural performances of steel-precast UHPC composite beams: Full-depth slabs with studs vs. demountable slabs with bolts, *Eng. Struct.* 260 (2022) 114230.
- [21] S.W. Yoo, J.F. Choo, Evaluation of the flexural behavior of composite beam with inverted-T steel girder and steel fiber reinforced ultra high performance concrete slab, *Eng. Struct.* 118 (2016) 1-15.
- [22] Specification for mix proportion design of ordinary concrete JGJ 55-2019. Beijing, China; 2019.
- [23] Reactive Powder Concrete GB/T 31387–2015. Beijing, China; 2015.
- [24] Standard for test methods of concrete physical and mechanical properties GB/T 50081-2019. Beijing, China; 2019.
- [25] T/CBMBF 37–2018, T/CCPA 7–2018, Fundamental characteristics and test methods of ultra-high performance concrete. Beijing, China; 2018.
- [26] Code for design of concrete structures GB 50010-2010. Beijing, China; 2010.
- [27] W.Z. Zheng, L. Li, Y. Wang, Compressive stress-strain relationship of steel fiber-reinforced reactive powder concrete after exposure to elevated temperatures, *Constr. Build. Mater.* 35 (C) (2012) 931-940.
- [28] Y.X. Ou, C.J. Shi, J.H. Shi, B. Shan, Z.M. Wu, Y. Huang, Y. Xing, Compressive mechanical properties and prediction for elastic modulus of ultra-high performance concrete, *J. Chinese Ceram. Soc.* 49 (2) (2021) 296-304. (in Chinese)
- [29] Metallic Materials-Tensile Testing-Part 1: Method of Text at Room Temperature GB/T 228-2010. Beijing, China; 2010.
- [30] P. Zhang, X.L. Lv, Y. Liu, X.X. Zou, Y.Z. Li, J.Q. Wang, S.A. Sheikh, Novel fiber reinforced polymers (FRP)-ultra high performance concrete (UHPC) hybrid beams with improved shear performance, *Constr. Build. Mater.* 286 (2021) 122720.
- [31] M. Singh, A.H. Sheikh, A.M.S. Mohamed, P. Visintin, M.C. Griffith, Experimental and numerical study of the flexural behaviour of ultra-high performance fibre reinforced concrete beams, *Constr. Build. Mater.* 138 (2017) 12-25.
- [32] P. Feng, H.L. Qiang, L.P. Ye, Discussion and definition on yield points of materials, members and structures, *Eng. Mech.* 34 (3) (2017) 36-46. (in Chinese)

- [33] Code for design of composite structures JGJ 138-2016. Beijing, China; 2016.
- [34] S.H. He, G. Yang, W.J. Zhou, Q.F. Li, Y. Dong, Evaluation of shear lag effect in HSS-UHPC composite beams with perfobond strip connectors: Experimental and numerical studies, *J. Constr. Steel Res.* 194 (2022) 107312.
- [35] P. Zhang, H. Liu, D.Y. Gao, J. Zhao, H. Feng, G.B. Tang, Shear-bond behavior of the interface between FRP profile and concrete by the double-lap push shear method, *J. Compos. Constr.* 21 (4) (2017) 04017012.
- [36] A. Kozma, Demountable Composite Beams: Analytical Calculation Approaches for Shear Connections with Multilinear Load-Slip Behaviour, Ph. D. Thesis, University of Luxembourg, Luxembourg, 2020.
- [37] W.J. Ge, Z.W. Zhang, Z.W. Guan, A. Ashour, Y. Ge, Y.W. Chen, H.B. Jiang, C.Z. Sun, S. Yao, W.H. Yan, D.F. Cao, Numerical study on flexural and bond-slip behaviours of GFRP profiled-concrete composite beams with groove shear connector, *Eng. Struct.* 275 (2023) 115226.
- [38] S. Muhammad, M. Takashi, K. Ko, Flexural behavior of reinforced concrete beams repaired with ultra-high performance fiber reinforced concrete (UHPFRC). *Compos. Struct.* 157 (2016) 448-460.
- [39] Z.Q. Dong, Z.Q. Liu, J.H. Ji, H. Zhu, X.X. Shao, G. Wu, Z.Q. Yang, Flexural behavior of small-sized I-shaped UHPC beams hybrid reinforced with steel plate and BFRP, *Compos. Struct.* 306 (2023) 116595.
- [40] M.X. Xu, X.W. Liang, P. Wang, Z.Y. Wang, Theoretical investigation on normal section flexural capacity of UHPC beams. *Eng. Mech.* 36 (8) (2019) 70-78. (in Chinese)